Preprint Cambridge Centre for Computational Chemical Engineering ISSN 1473 – 4273

Modelling a detailed kinetic mechanism for electrocatalytic reduction of CO_2

Simon D. Rihm [1,2,3],

Jethro Akroyd [1,2], Markus Kraft [1,2,4]

released: January 20, 2022

[1] Department of Chemical Engineering
and Biotechnology
University of Cambridge
Philippa Fawcett Drive
Cambridge, CB3 0AS
United Kingdom

E-mail: mk306@cam.ac.uk

[2] CARES
Cambridge Centre for Advanced
Research and Education in Singapore
1 Create Way
CREATE Tower, #05-05
Singapore, 138602

[3] Department of Chemical &
Biomolecular Engineering
National University of Singapore
4 Engineering Drive 4
Singapore, 117585.

[4] School of Chemical
and Biomedical Engineering
Nanyang Technological University
62 Nanyang Drive
Singapore, 637459

Preprint No. 289

Keywords: Micro-Kinetic Model, Reaction Mechanism Generation, CO2 Reduction Reaction, Fuel Synthesis, Electrolysis, Copper Electrocatalyst, Carbon Utilization

Edited by
Computational Modelling Group
Department of Chemical Engineering and Biotechnology
University of Cambridge
Philippa Fawcett Drive
Cambridge CB3 0AS
United Kingdom

E-Mail: c4e@cam.ac.uk
World Wide Web: http://como.ceb.cam.ac.uk/

Abstract

For the first time a fully-elementary reversible kinetic model for electrocatalytic CO_2 reduction towards a multitude of different products has been established and verified with experimental data. The detailed reaction mechanism was generated by compiling hypothesized reaction paths and intermediates from many different sources. Thereby a focus was put on distinguishing different embodiments of similar elementary steps: For proton-coupled electron transfer three hydrogenation mechanisms were considered and for intermediates with unclear molecular structure separate paths were modelled. The micro-kinetic model was fed with tabulated energy parameters and results of Density Functional Theory (DFT) calculations to simulate CO_2 reduction on a Cu(100) surface for constant applied potentials. The operating conditions were chosen according to published experimental results in order to compare Faradaic Efficiencies. With these, the model parameters were successfully calibrated across a wide potential range while keeping all values within a tight interval of theoretical bounds derived from ab initio calculations and other theoretical considerations. The calibrated model was found to be in good agreement with the measurement data and also captures qualitative trends of surface coverages reported for in-situ measurements. Most interestingly, it finds the widely accepted hypothesis of dimerization via $*CO$ intermediates to be inaccurate. Instead, coupling reactions of $*CHO$ and $*CH_2$ intermediates are observed. The shifting of dimerization routes with varying applied potential – especially towards ethylene – is supported by other experimental studies. Furthermore, this work establishes a methodology of creating and calibrating complex electrochemical micro-kinetic models.

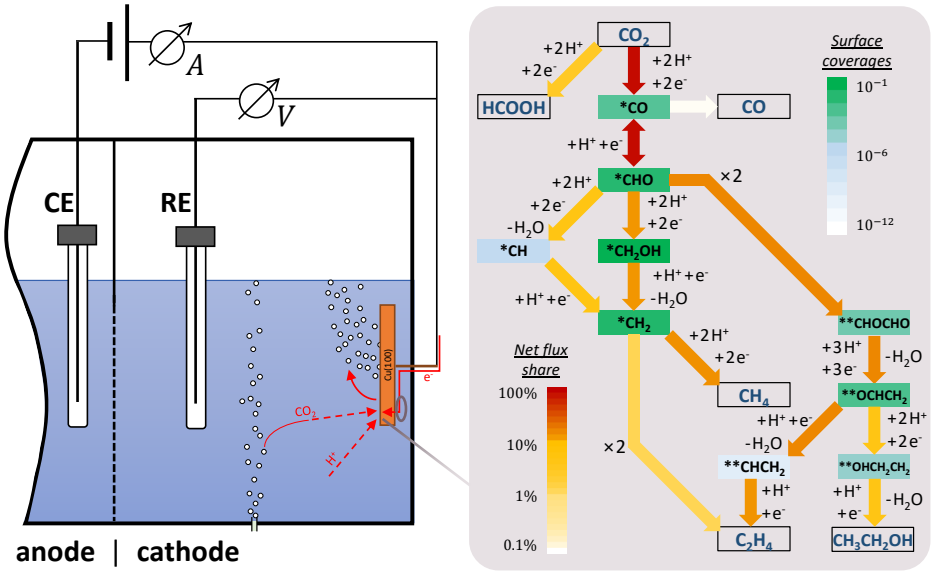

Highlights

- First fully reversible kinetic model towards multiple products
- Model successfully calibrated for experimental results
- Methodology of creating and calibrating complex electrochemical MKM
- Flux analysis indicating coupling reactions without adsorbed CO

Contents

1 Introduction

The electrochemical reduction of CO_2 to hydrocarbons is a promising pathway to convert renewable energy into fuels and commodity chemicals. Copper-based electrodes can produce a wide variety of valuable products such as ethylene and ethanol [20]. These have therefore been the most intensely studied electrocatalysts and immense progress has been made in engineering electrodes with high Faradaic Efficiencies [8].

Increasing efficiencies for valuable products remains the critical barrier towards economic feasibility and commercialisation. Besides process conditions and applied potential, experimental studies have shown surface structure and morphology to be key parameters in this effort [28]. For systematic optimization a deeper understanding of the fundamental processes is needed though - especially the mechanism of dimerization remains an ongoing topic of discussion.

Key to this understanding is the investigation of the CO_2 Reduction Reaction (CO2RR) on copper single-crystal surfaces. This is usually done by applying a constant potential to the working electrode for a prolonged time while keeping the CO_2 concentration stable. After a while, a steady current can be measured that is driving constant product synthesis. For each product the so-called Faradaic Efficiency can now be calculated that indicates the fraction of total current utilized towards a certain product. The aim is to increase this fraction for valuable products such as ethylene and decrease it for unwanted products such as hydrogen that is produced via the competing Hydrogen Evolution Reaction (HER). Cu(100) has been found to favour ethylene production the most [33].

In this study we focus on some specific measurements of this kind carried out by Huang and co-workers on Cu(100) for different applied potentials [15]. A simplified schematic of their three-electrode setup is shown in Fig. 1. They used a pH-neutral potassium bicarbonate solution through which CO_2 was constantly bubbled to ensure saturation. For 40 minutes at a time, constant potentials were applied between the reference and the working electrode while the current between working and counter electrode was measured. Gaseous products were then building up in the headspace and liquid products in the electrolyte, both of which were sampled and measured quantitatively by adequate methods. Finally, the applied potentials were converted to refer to the Reversible Hydrogen Electrode (RHE) and calculated Faradaic Efficiencies were reported for each.

These experimental studies alone unfortunately do not convey all desired insights due to the large number of possible intermediates and reaction paths. For this reason, numerous ab initio studies have been done on postulated reaction paths for certain catalyst surfaces [11, 12, 22–24, 26, 27]. These usually report Gibbs Free Energies ΔG, activation energies E_{act} or both, for each elementary reaction step. Based on their orders of magnitude, assessments regarding the limitations of the reaction are made. The explanatory power of these is limited for three reasons: First, they usually focus on an extract or simplified version of the reaction mechanism. Second, kinetics depend on potentials applied to the catalyst and reaction paths are known to shift across rather small voltage ranges. Third, reaction rates also depend on intermediate surface coverages which are subject to transient changes in the reactor.

Even though recent studies and reviews give a more complete picture by looking at many

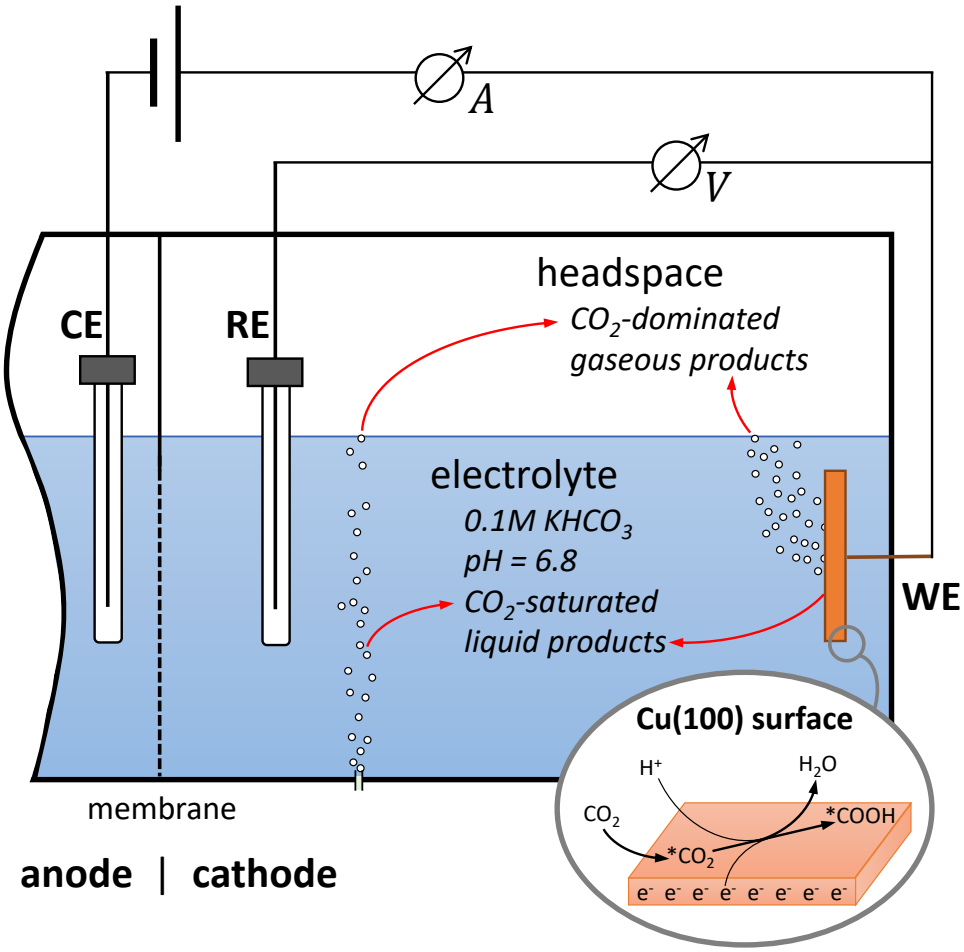

Figure 1: *Schematic of the electrode setup based on a widely used electrochemical cell design [20, 31] showing a working electrode (WE), counter electrode (CE) and reference electrode (RE) within a CO_2-saturated electrolyte. The CO2RR occurs at the copper WE within the cathodic section.*

different full reaction paths and document potential-dependent activation barriers as well Gibbs Free energies [3, 18, 28], the problem remains that verifiable assessments can be rarely made due to the complexity of the reaction mechanism. These limitations can be overcome by a micro-kinetic model (MKM) that simulates the transient reaction behaviour. The rates of all relevant elementary reactions are calculated for each timestep and integrated so that surface coverages and production rates can be gathered. So far, this has only been done for selected portions of the mechanism, towards selected products or with steps and products lumped together [12, 23, 38].

The purpose of this paper is to report a full micro-kinetic model that can help understand the CO2RR mechanism better and give a basis for future reactor optimisation. Notably, all steps and parameters involved are based on existing experimental work and ab initio studies. The methodology developed showcases the potential of applying core capabilities of the combustion community to emerging fields as highlighted by Robert Kee in 2016 [16].

2 Methodology

2.1 Elementary kinetic modelling

A general elementary reaction i can be written as

$$\sum_k \nu'_{ki} \chi_k^{z_k} \rightleftharpoons \sum_k \nu''_{ki} \chi_k^{z_k}, \tag{1}$$

where $\chi_k^{z_k}$ is the participating species with charge z_k, while ν'_{ki} and ν''_{ki} are the stoichiometric coefficients.

Each species is assigned an activity concentration $C_{\mathrm{ac},k}$, chemical potential μ_k and an electric potential Φ_k. Activity concentration is defined as

$$C_{\mathrm{ac},k} = \gamma_k C_k = a_k C^\circ. \tag{2}$$

where activity a and activity coefficient γ show deviations of behaviour from a well-defined reference state.

The thermodynamic equilibrium condition is defined by $\Delta G_i = 0$ (for reaction i) and can be written as

$$\Delta G^\ominus + RT \ln \left(\prod_{k=1}^{K} a_k^{\nu_{ki}} \right) + \sum_k \nu_{ki} z_k F \Phi_k = 0. \tag{3}$$

where $\Delta G^\ominus = \sum_k \nu_{ki} \mu_k^\ominus$. Thus, the equilibrium constant is

$$K_i = \prod_{k=1}^{K} a_k^{\nu_{ki}} = K_i^t \exp\left(-\frac{\sum_k \nu_{ki} z_k F \Phi_k}{RT} \right). \tag{4}$$

Note that for non-electrochemical reactions, the equilibrium constant is simply $K_i^t = \exp(-\Delta G_i^\ominus / RT)$.

The rate of progress for elementary reactions is given as

$$q_i = k_{\mathrm{f}i} \prod_{k=1}^{K} (C_{\mathrm{ac},k})^{\nu'_{ki}} - k_{\mathrm{r}i} \prod_{k=1}^{K} (C_{\mathrm{ac},k})^{\nu''_{ki}}, \tag{5}$$

where $k_{\mathrm{f}i}$ and $k_{\mathrm{r}i}$ are the forward and reverse reaction rate constants for reaction i that generally follow the Arrhenius form in Eq. (6),

$$k_{\mathrm{f}i}^t = A \exp\left(-\frac{\mathrm{E_{act}}}{RT} \right). \tag{6}$$

For electrochemical reactions, activation barriers shift with applied potential which can be computed via Marcus theory [38]. We will not look at barriers on the level of reorganization energies in this paper and represent the relationship between the activation energy

and the applied electrode potential by a constant charge transfer coefficient β:

$$\beta = \frac{\beta'}{nF} = -\frac{RT}{nF}\frac{\partial \ln k}{\partial U} = -\frac{1}{nF}\frac{\partial E_a}{\partial U}, \tag{7}$$

where n is the number of electrons transferred. The forward rate constant $k_{\mathrm{f}i}$ is now given by

$$k_{\mathrm{f}i} = k_{\mathrm{f}i}^{t} \exp\left(-\beta_{\mathrm{f}i}' \sum_k \frac{\nu_{ki} z_k F \Phi_k}{RT}\right). \tag{8}$$

With the kinetic condition for equilibrium, $q_i = 0$, the reverse reaction rate constant can be calculated from Eqs. (2), (5), (8) and (4). Each elementary reaction therefore requires an activation barrier $\mathrm{E_{act}}$, a Gibbs Free energy $\Delta \mathrm{G}^{\ominus}$ and a pre-exponential factor A. Electrochemical reactions additionally require a charge transfer coefficient β.

2.2 Mechanism Generation

There are three basic and two advanced types of elementary reactions to consider within the CO2RR mechanism:

1. **Adsorption and Desorption** steps include the transition between surface-bound intermediates and educts or products in the bulk. Initial adsorption of CO_2 can happen via physisorption or chemisorption which we differentiate by electron transfer.

2. **Hydrogenation** steps are generally the way of reducing the carbon towards our products by transferring an electron from the electrode and a proton from the electrolyte to the intermediate. Depending on their sequencing and the proton orgin, there are a multitude of different options how this "Proton-coupled Electron Transfer" can happen.

3. **Coupling** steps initiate the dimerization necessary for C_2 products and are crucial for our understanding of the mechanism. We focus entirely on Langmuir-Hinshelwood type reactions, some of which are mixed-species and some of which are same-species.

4. *Other* reaction types are for example isomerization steps of re-structuring intermediates.

5. *Combined* reactions are also possible when adsorption or desorption is directly tied to a hydrogenation or coupling step - for example as associative desorption.

Countless studies have been published on the CO2RR mechanism on copper-based catalysts. We have derived a detailed and coherent mechanism towards C_1 and C_2 products as well as for HER based on these criteria: Inclusion of often-reported steps, inclusion of often-reported products, availability of ab intio results. The full mechanism includes 77

steps and is reported in the Supplementary Material. In total, 9 products are included: 3 two-electron products (H_2, CO, HCOOH), 3 multi-electron C_1 products (CH_4, CH_3OH, CH_2O) and 3 C_2 products (C_2H_4, CH_3CH_2OH, CH_3COOH).

The modelling of hydrogenation reactions is key as they are the ones mainly driven by applied potential. Mechanistically, we assume proton and electron transfer to be simultaneous and not sequential. For each of these steps we included three mechanisms that can be distinguished by proton origin and we named after their equivalent counterparts in the HER:

1. "Acidic" is the standard Eley-Rideal type hydrogenation via concerted transport of an electron and H^+ ion: $*A + H^+ + e^- \rightleftharpoons *B$
2. "Heyrovsky" is another Eley-Rideal type hydrogenation via concerted transport of an electron and water as proton origin: $*A + H_2O + e^- \rightleftharpoons *B + OH^-$
3. "Tafel" is a Langmuir-Hinshelwood type surface hydrogenation via an adsorbed proton on the surface: $*A + *H \rightleftharpoons *B + *$

2.3 Model Calibration

The MKM has over 300 distinctive parameters that all influence the system response when a potential is applied. Calibrating the model is basically a multi-objective optimization task where we need to find an optimum within the parameter hyperspace regarding the following main objectives:

1. Trueness to ab initio calculations
2. Thermodynamic consistency (conservation of energy throughout the mechanism)
3. Reproducing qualitative and quantitative findings from experiments

We approached this by coming up with objective functions that incorporate these, selecting a set of parameters to adjust and deploying the Hooke Jeeves algorithm - analogous to an approach reported for a similar calibration task [2]. We divided the parameters into groups and focused on two of the three objectives at a time.

We came up with a strategy that breaks the calibration down into three parts: In the first part, chemical potentials are optimized for the system to get as close as possible to DFT-derived values while thermodynamic consistency is a boundary condition. In the second part, activation barriers and charge transfer coefficients are optimized towards logarithmically scaled Faradaic Efficiencies while they are allowed to vary in a small range around target values. In the last part, pre-exponential factors are optimized towards linearly scaled Faradaic Efficiencies.

3 Results

First, all the chemical potentials of involved species were calibrated. We can report a coherent and self-consistent reaction network with Gibbs free energies and potentials deviating less than 0.08 eV from their tabulated or reported values on average. They all lie within their individually defined uncertainty ranges.

Subsequently, all kinetic parameters were calibrated in multiple steps. They also all lie within their tightly defined boundaries. The resulting model can predict Faradaic Efficiencies of the three major products (H_2, CH_4, C_2H_4) with high accuracy. When it comes to the minor products, we found good experimental agreement for three of them (CO, HCOOH, CH_3CH_2OH) but poor agreement for the remaining three (CH_3COOH, CH_2O, CH_3OH) - the latter two of which were not detected at all in the considered experiments [15].

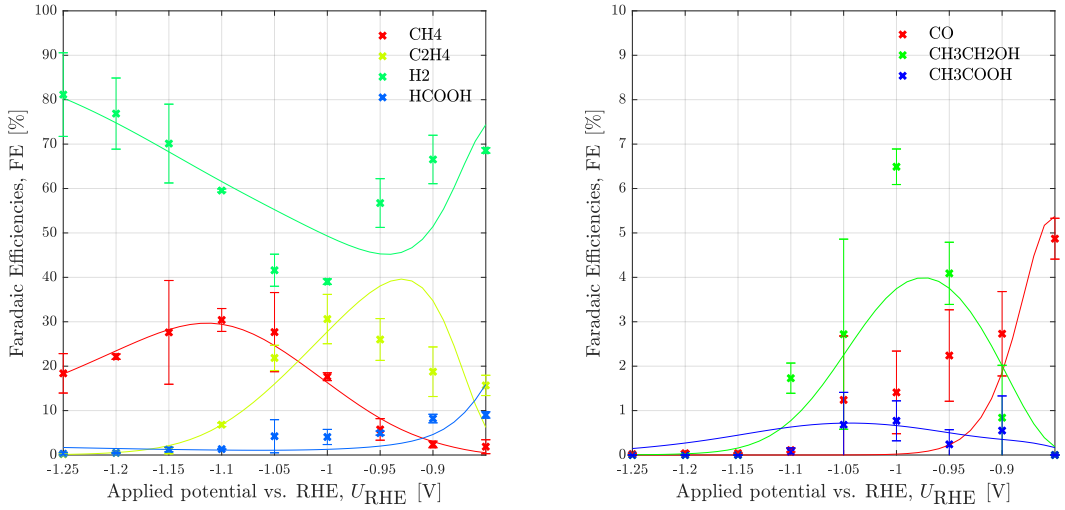

(a) Major products

(b) Minor products

Figure 2: *Faradaic Efficiencies produced by the final MKM (calibrated and extended by bulk reactions).*

Acetic acid production was not achieved by the MKM with any of the over 30,000 tested parameter combinations. Since the formation of carboxylic acid groups within the CO2RR mechanism is still very unclear, we considered possible reactions subsequent to the electrocatalysis: Cannizzaro reactions have been proposed before [28] and many other bulk reactions like hydrolysis of ketene are also a possibility. We finally chose carbonylation of methanol as a realistic surrogate: $CO + CH_3OH \longrightarrow CH_3COOH$. We assumed it to use residual carbon monoxide that was dissolved in the electrolyte and adjusted Faradaic Efficiencies accordingly.

Furthermore, we assumed the volatile formaldehyde to be depleted by subsequent reactions. It is readily oxidized by atmospheric oxygen so we included $2\,CH_2O + O_2 \longrightarrow 2\,HCOOH$ via residual oxygen in the electrolyte or the headspace. The final results of our calibrated and extended MKM compared to experimental data are shown in Fig. 2.

4 Discussion

The biggest advantage of having a calibrated and fully functioning MKM is that we are now able to analyse the reaction paths by looking at individual reaction rates and surface coverages. In Fig. 2 we show a flux diagram for the full reaction mechanism after 40 minutes of applying −1 V. Each step in the mechanism is represented by an arrow with the unique reaction ID and indications of absolute and relative reaction rates. The bulk reactions by which we extended our model and adjusted Faradaic Efficiencies are not included. We purposefully chose a medium voltage to show the low-potential as well as the high-potential trends.

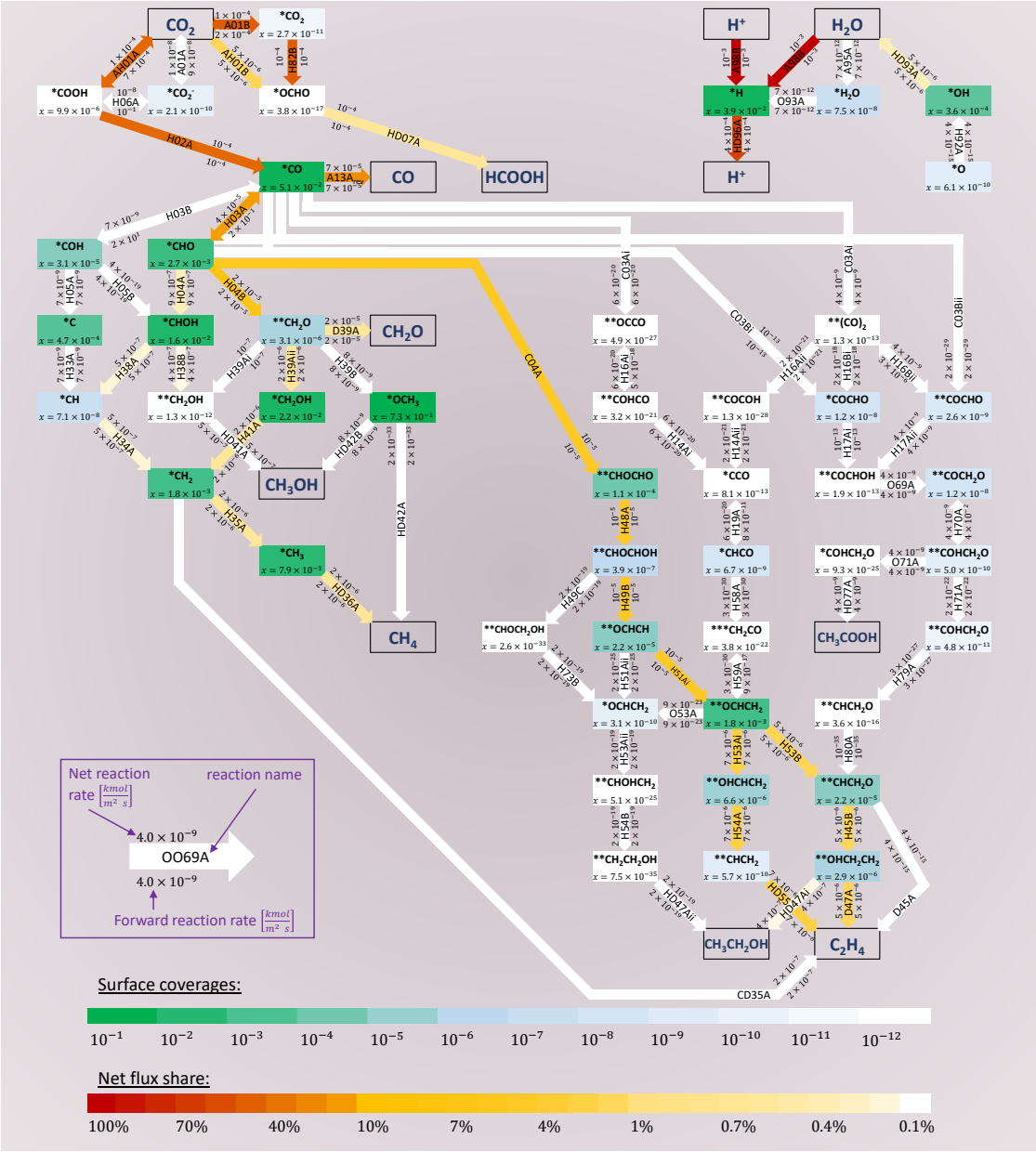

(a) $U = -0.85\,\mathrm{V}$

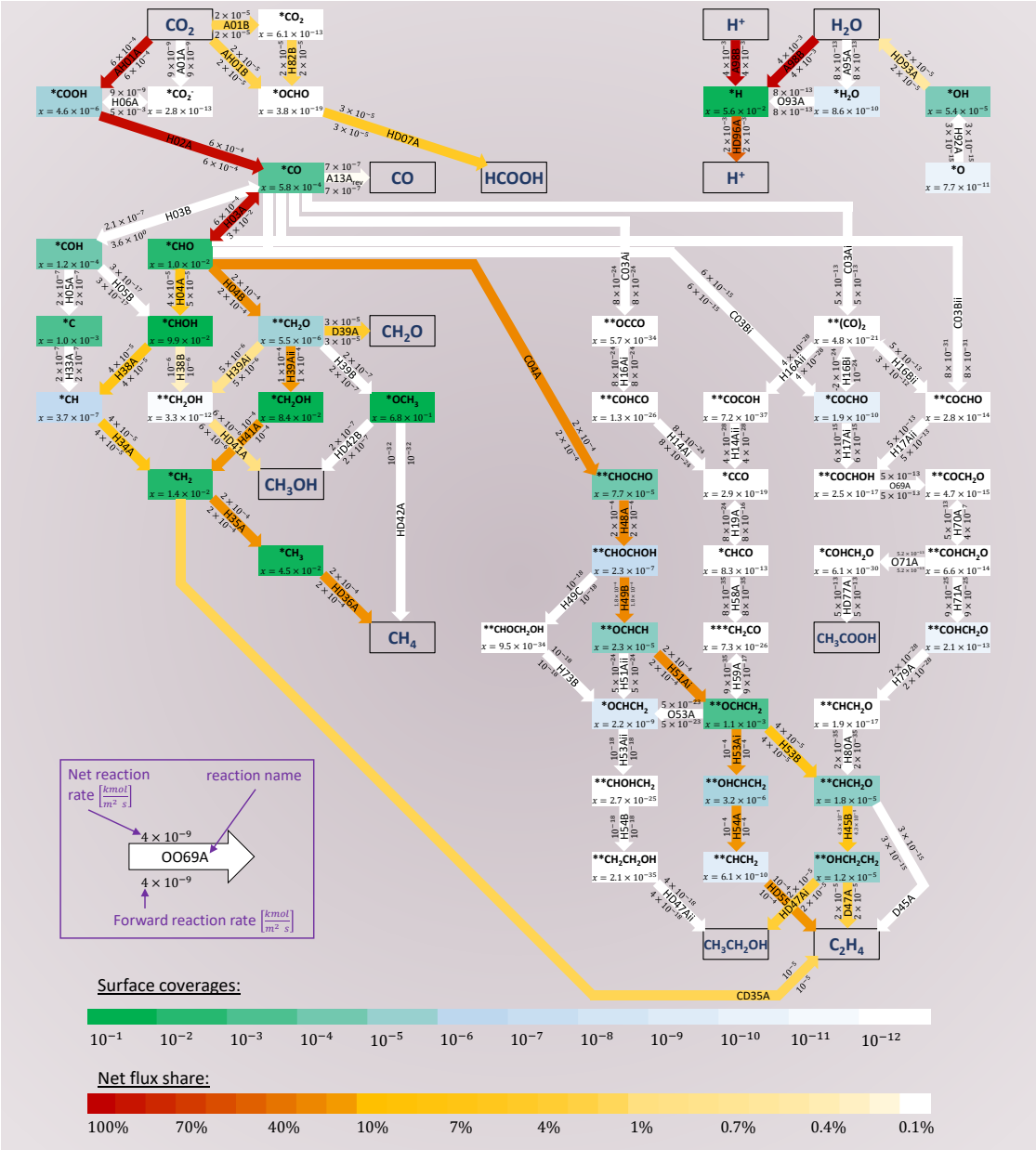

(b) $U = -1.00\,\mathrm{V}$

A few caveats apply: Coupling reactions naturally occur at maximum half the rate of reaction towards one of the monomers. Also, CO2RR reactions are relative to initial CO_2 adsorption while HER reactions are relative to inital proton adsorption. And since the flux diagram does not differentiate between the hydrogenation modes, two effects come into play when comparing flux towards and from $*$H. First of all, some of the adsorbed protons are used for other hydrogenation reactions, creating a second net stream away from $*$H. Second, Tafel reaction is like a coupling reaction and therefore at maximum half the flux of proton adsorption while the other hydrogenation mechanisms can occur at the same flux theoretically.

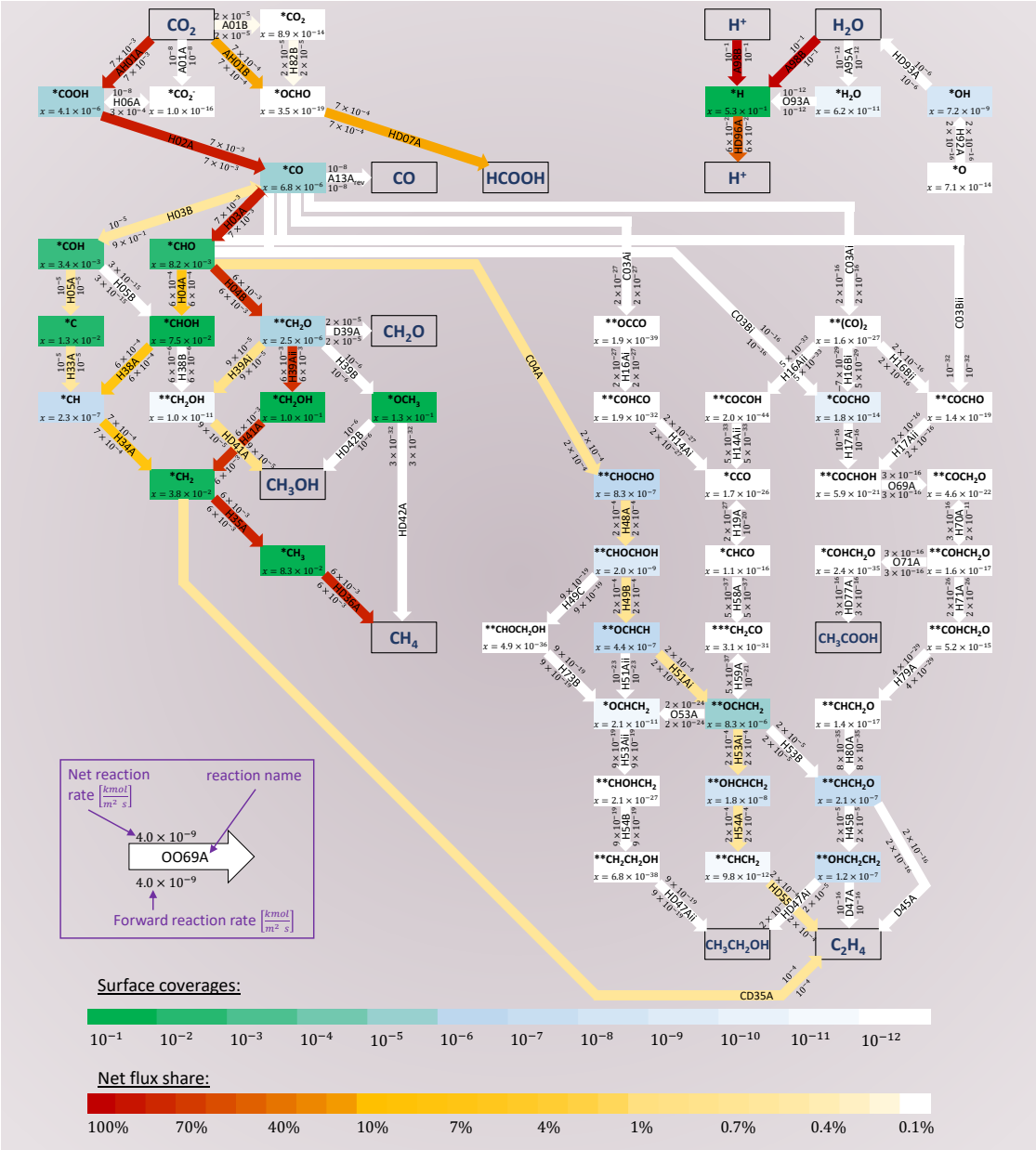

(c) $U = -1.15\,\mathrm{V}$

Figure 2: *Flux Diagram of the MKM reaction mechanism after* $t = 2400\,\mathrm{s}$ *for appplied constant potentials* U*. Intermediate coverages are indicated by the green-blue-white scale (logarithmically) of the species boxes. The share of each reaction in the whole mechanism (in relation to overall CO2 adsorption for CO2RR and to proton adsorption for HER) is indicated by the red-yellow-white scale (semi-logarithmically) of the reaction arrows. If the reverse reaction rate is at more than 1% of the forward reaction rate, this was indicated by an equilibrium arrow. The size of the reverse arrow relative to the forward arrow indicates the ratio of reverse reaction rate to forward reaction rate.*

The most obvious observation from studying flux diagrams is the fact that while most of the steps in the HER and C1-CO2RR mechanism become active, large parts of the C2-CO2RR are mostly inactive - which they continue to be throughout the range of applied potential. This is mostly due to the fact that the only significant coupling reactions seem to be $*CHO$ or $*CH_2$ dimerization while - contrary to many hypotheses published over the last years [11, 17, 25] - $*CO$ is not directly involved in coupling reactions at all. Further downstream, the reaction path towards acetic acid proposed by Garza and co-workers [11] is also not active. These findings were qualitatively the same for all considered parameter sets from beginning to end of the kinetic calibration process.

There is a critical debate about the feasibility of $*CO + *CO$ coupling - represented by reactions "C03Ai" and "C03Aii" - on Cu(100) surfaces: While some authors claim this pathway exists even at low potentials [11], others argue the reaction barrier is too large on this specific copper facet [12]. A widely accepted middle-way is a mixed coupling step of $*CO + *CHO$ - represented by reactions "C03Bi" and "C03Bii" - [11, 12, 23, 35], but these aren't energetically feasible in our model either. Much of the reasoning for $*CO$ involvement in coupling reactions is the assumption that coverages of other intermediates are too low [11]. But Fig. 2 shows that even a $100\times$ larger surface concentration can be offset by a $\approx 0.4\,\mathrm{eV}$ larger activation barrier.

For this reason, we included surface coverages of the intermediates in the flux diagram. Flux alone is not enough to make judgement about limiting steps since the depicted mechanism is already in a quasi-equilibrium so if a certain step in a path of the reaction network is limiting, the whole path would appear to be inactive from the point of branching on. Here, the coupling reactions seem to be actually rate- and selectivity-limiting since the monomer coverage is much higher than that of the corresponding dimers $**OCCO$ and $**(CO)_2$. On the other side, the mixed coupling dimers $*COCHO$ and $**COCHO$ are much more abundant than their common downstream product, $**COCHOH$. This suggests that the acetic acid pathway's inactivity is not only caused by the prior coupling reactions but also thermodynamic and kinetic inhibition within the path after coupling. Another such example is $**COCH_2O$, which makes reactions "H17Ai", "H17Aii" and "H70A" prime candidates as rate-limiting steps towards CH_3COOH. Since the activation barrier values of these are already in the lower parts of their allowed ranges, this suggests that the proposed acetic acid pathway is not feasible on Cu(100) catalysts. The possible bulk reactions speculated earlier could explain this behaviour without an isomerism to shift a second oxygen from one carbon to the other.

For larger applied potentials, the reaction paths start to shift and - amongst others - the $*CH_2 + *CH_2$ coupling reaction "CD35A" - which has also been suggested for a long time [14, 34] - becomes active. This corresponds well with the "Low-Potential Ethylene and Ethanol Path" and the "High-Potential Methane and Ethylene Path" proposed by Luo and co-workers [24]. Since many of our parameter target values are derived from ab initio results by the same group, some confirmation bias might be at play here. But since we also considered DFT results from numerous other publications and relied on actual measurements for calibration, these findings are still meaningful. It also supports the hypothesis established by Koper and co-workers that Cu(111) and Cu(100) both show a pathway towards ethylene which has a common intermediate with the formation of methane but only Cu(1000) has a second pathway towards ethylene that is active at relatively low applied

potentials [33].

Besides the net flux of each reaction, its sensitivity to minor changes is of interest. For this reason, we also looked at the absolute forward reaction rate and compared it to the net reaction rate. If the two are almost the same, no notable reverse reaction is taking place. If the forward reaction rate is considerably larger, there is a reverse reaction occuring at a similar rate which makes the net rate very susceptible to small changes in coverages and energies. This is apparent in Fig. 2 especially for initial adsorption and hydrogenation of CO_2 up to CO and HCOOH. The equilibria of these steps shift drastically over the range of applied potential so that most of the steps are active at some point. We have based the separation of $*CO_2$ and $*CO_2^-$ pathways towards CO and HCOOH respectively on multiple publications [3, 10, 35]. We also included the combined adsorption and hydrogenation steps as proposed many times throughout the literature [18, 21, 27]. For HCOOH production, the physisorption route is dominant for small applied potentials and the direct route becomes only feasible at higher potentials. The two-step route to *COOH with decoupled electron and proton transfer is not active in our simulations, but this is probably caused by the implementation: The full potential drop is assumed to occur between the catalyst surface and the electrode which leads applied potential to only speed up proton transfer.

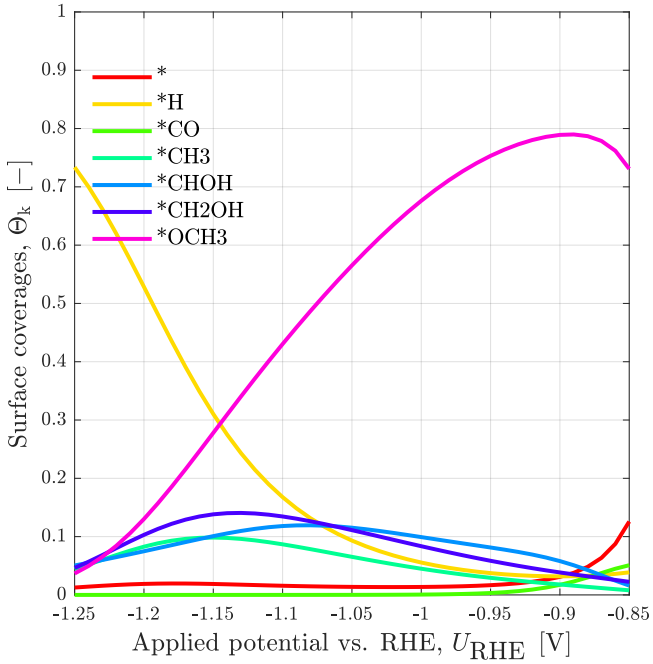

Figure 3: *Surface coverages after* $t = 2400\,\mathrm{s}$ *simulated by the calibrated MKM*

Surface-bound carbon monoxide as a key intermediate is described in many publications: Models by Goodpaster [12] and Luo [24] predicted a *CO dominated Cu(100) surface that is only interrupted by a *H peak between 0.0 V and −0.5 V. These models only consider competitive adsorption between the two intermediates though and assume a downhill reaction path from there. This is contradicted by experimental findings of Wuttig and coworkers [37] that only found a *CO signal from −0.6 V onwards, peaking around −0.8 V

during in-situ measurements. Our simulations seem to agree with this since Fig. 3 shows adsorbed carbon monoxide can be found in larger quantities still around $-0.85\,\mathrm{V}$, going down sharply for larger applied potentials. The adsorbed proton coverage only rises at very large applied potentials which indicates the overwhelmingly strong HER at this point.

Birdja and co-workers [3] describe further findings via in-situ SEIRAS, IRAS and SERS. A few weaker bands were also detected that can be attributed to $*$CHO for example. Indeed, we see a few other C_1 intermediates with an oxygen that at least for lower applied potentials show coverages well below $x_{*\mathrm{CO}}$. Moreover, a dimer with two different C-O stretching frequencies was found on copper single-crystal electrodes within alkaline media [3]. Since our simulations don't show dimers with a coverage large enough to display in Fig. 3, we have to look at the flux diagrams in Fig. 2 once again. The only such intermediate would be $**$CHOCHOH but there are multiple C_2 intermediates with significantly larger coverages. This either detracts from our model, has systematic reasons, or implies that $**$CHOCHO structure is not as symmetrical as we assumed.

The dominant $*OCH_3$ intermediate is not described anywhere which is likely due to shortcomings in our model but could also have other reasons. More interestingly, even within the confines of our model this is not a key intermediate mechanistically despite its large coverage. On the contrary, it acts more like a catalyst posion since this reaction path is a very slow "dead end". This shows that - at least in theory - the CO2RR mechanism can poison itself in certain conditions which could be a factor that drives catalyst aging.

Overall, we find absolute values of surface coverages to be much less critical for and indicative of the mechanism than originally assumed.

5 Conclusion

We present the first fully-elementary CO2RR kinetic model with nine products via many different reaction paths. The parameters are strongly tied to DFT calculation results and were calibrated successfully towards experimental data across a substantial range of applied potentials. We also find good qualitative agreement with observations and hypotheses reported in other studies. The model quality can be determined by these since only the quantitative data set been used for the actual calibration.

A thorough flux analysis has been done with the calibrated model for the reaction mechanism in action. We report a few key findings regarding the CO2RR mechanism on Cu(100): We find no involvement of $*$CO in the coupling reaction despite heightened coverage, but two other routes via $*$CHO and $*CH_2$. At the same time, we cannot see any substantial acetate production via any of the reported reaction paths and conclude bulk reactions coming into play. Our model is less accurate for smaller overpotentials and - if extrapolated beyond the potential range used for calibration - shows large formate production - similar to what Xiang and co-workers [38] reported for their model. The initial steps of CO2RR and HER and their interplay as competitive adsorption would need parameter adjustment to extend viability of the model beyond the reported scope.

We also came up with a robust methodology for mechanism generation, parameter assess-

ment and model calibration that can be applied to other micro-kinetic models for CO2RR and even other electrocatalytical processes. From an analysis and benchmarking perspective, we suggest reporting all elementary steps and intermediates together with their respective parameters. Moreover, flux diagrams should be shown for key conditions in combination with coverages and sensitivities of reaction rates.

Going forward, there are three main directions of interest: First of all, we aim to extend the existing model so we can include more products and essential reaction steps. Secondly, calibrating the model to a wider range of operating conditions such as temperature, pH or applied potential. Finally, similar models for different surface facets can be produced and compared amongst each other to work towards a complete model for polycrystalline copper.

Acknowledgements

This research was supported by the National Research Foundation, Prime Minister's Office, Singapore under its Campus for Research Excellence and Technological Enterprise (CREATE) programme. S. D. Rihm acknowledges financial support from Fitzwilliam College Cambridge and the Cambridge Trust. M. Kraft gratefully acknowledges the support of the Alexander von Humboldt Foundation.

Nomenclature

Upper-case Roman

A	Pre-exponential (Arrhenius) factor
C	Concentration
C_{ac}	Activity concentration
$\mathrm{E_{act}}$	Activation barrier/energy
F	Faraday constant
$\Delta\mathrm{G}$	Gibbs Free Energy of a reaction
K	Equilibrium constant of a reaction
R	Universal Gas constant
T	Temperature
U	Applied potential

Lower-case Roman

a	Activity of a species
k	Reaction rate coefficient
n	Number of electrons transferred
q	Rate of progress for a reaction
z	Charge of a species

Upper-case Greek

Φ	Electric potential

Lower-case Greek

β	Charge Transfer Coefficient
γ	Activity Coefficient
μ	Chemical potential
ν	Stochiometric coefficient
χ	Generic chemical species

Superscripts

$\circ$	Reference state
$\ominus$	Standard state
t	Thermal-only

Subscripts

f	forward reaction
i	Reaction control variable
k	Species control variable
r	reverse reaction

Abbreviations

CEP	Constant Electrode Potential
CHE	Computational Hydrogen Electrode
CO2RR	CO_2 Reduction Reaction
CREATE	Campus for Research Excellence and Technological Enterprise
DFT	Density Functional Theory
FE	Faradaic Efficiency
HER	Hydrogen Evolution Reaction
IRAS	Infrared Reflection Absorption Spectroscopy
MKM	Micro-kinetic Model
OF	Objective Function
PEF	Pre-exponential factor
PMF	Potential of Mean Force
RHE	Reversible Hydrogen Electrode
SEIRAS	Surface-enhanced Infrared Absorption Spectroscopy
SERS	Surface-enhanced Raman Spectroscopy

A Reaction mechanism used for micro-kinetic model

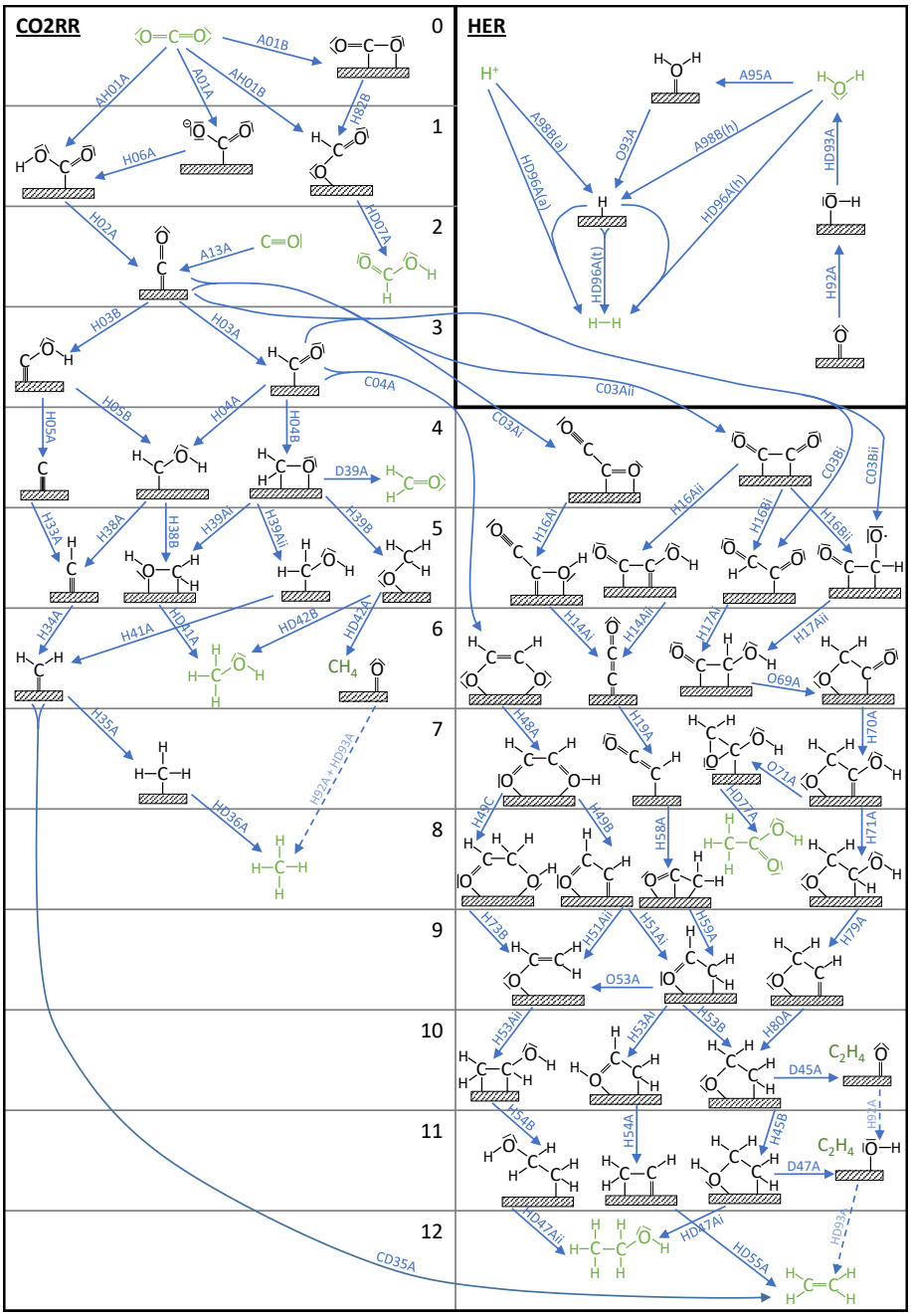

Figure 4: *Reaction network of mechanistic pathways included in the micro-kinetic model. For the CO2RR we used the tabular form of representation established by Nitopi et al. [28] where C_1 / C_2 species are on the left / right respectively and the rows from 0 to 12 indicate number of electrons transferred. Bulk species are depicted in green, surface-bound intermediates in blue. Names given on reaction arrows correspond to IDs in Tab. 1. Different hydrogenation steps are included explicitly for HER but not CO2RR.*

Fig. 4 depicts the full reaction mechanism used for the MKM. In Tab 1 all shown reactions are listed. The ID prefixes are based on reaction types: "H" for hydrogenation, "A" for adsorption, "D", for desorption, "C" for coupling, "O" for other and combinations of these accordingly. Hydrogenation reactions are usually included with multiple proton-transfer mechanisms for which the following replacements are performed:

1. In **acidic** hydrogenation, p^+ is a proxy for H^+. Reactions are suffixed by "(a)".
2. In **Heyrovsky** hydrogenation, p^+ is replaced by H_2O and an OH^- is added on the product side. Reactions are suffixed by "(h)".
3. In **Tafel** hydrogenation, $p^+ + e^-$ is replaced by $*H$. Reactions are suffixed by "(t)".

Table 1: *List of all reaction steps of the CO2RR mechanism considered in the MKM. Hydrogenation steps are only listed once even if they are effectively multiple reactions which is indicated in the respective columns on the right.*

Nr.	id	reaction	Tafel	alkaline	acidic
1	A98B	$* + e^- + p^+ \rightleftharpoons *H$	no	yes	yes
2	A95A	$* + H_2O \rightleftharpoons *H_2O$	no	no	no
5	O93A	$*H_2O + e^- \rightleftharpoons *H + OH^-$	no	no	no
8	HD96A	$e^- + p^+ + *H \rightleftharpoons H_2 + *$	yes	yes	yes
10	AH01A	$* + e^- + p^+ + CO_2 \rightleftharpoons *COOH$	yes	yes	yes
11	A13A	$* + CO \rightleftharpoons *CO$	no	no	no
12	H02A	$e^- + p^+ + *COOH \rightleftharpoons *CO + H_2O$	yes	yes	yes
14	A01A	$* + CO_2 + e^- \rightleftharpoons *CO_2^-$	no	no	no
15	H06A	$p^+ + *CO_2^- \rightleftharpoons *COOH$	no	yes	yes
18	A01B	$* + CO_2 \rightleftharpoons *CO_2$	no	no	no
19	AH01B	$* + e^- + p^+ + CO_2 \rightleftharpoons *OCHO$	yes	yes	yes
20	H82B	$e^- + p^+ + *CO_2 \rightleftharpoons *OCHO$	yes	yes	yes
22	HD07A	$e^- + p^+ + *OCHO \rightleftharpoons HCOOH + *$	yes	yes	yes
24	H03B	$e^- + p^+ + *CO \rightleftharpoons *COH$	yes	yes	yes
25	H05A	$e^- + p^+ + *COH \rightleftharpoons *C + H_2O$	yes	yes	yes
26	H33A	$e^- + p^+ + *C \rightleftharpoons *CH$	yes	yes	yes
27	H34A	$e^- + p^+ + *CH \rightleftharpoons *CH_2$	yes	yes	yes
28	H35A	$e^- + p^+ + *CH_2 \rightleftharpoons *CH_3$	yes	yes	yes
29	HD36A	$e^- + p^+ + *CH_3 \rightleftharpoons CH_4 + *$	yes	yes	yes
30	H03A	$e^- + p^+ + *CO \rightleftharpoons *CHO$	yes	yes	yes
31	H04B	$* + e^- + p^+ + *CHO \rightleftharpoons **CH_2O$	yes	yes	yes
32	D39A	$**CH_2O \rightleftharpoons CH_2O + 2*$	no	no	no
34	H04A	$e^- + p^+ + *CHO \rightleftharpoons *CHOH$	yes	yes	yes
35	H39Ai	$e^- + p^+ + **CH_2O \rightleftharpoons **CH_2OH$	yes	yes	yes
36	H39Aii	$e^- + p^+ + **CH_2O \rightleftharpoons *CH_2OH + *$	yes	yes	yes
37	H38A	$e^- + p^+ + *CHOH \rightleftharpoons *CH + H_2O$	yes	yes	yes
38	H38B	$* + e^- + p^+ + *CHOH \rightleftharpoons **CH_2OH$	yes	yes	yes
39	H39B	$e^- + p^+ + **CH_2O \rightleftharpoons *OCH_3 + *$	yes	yes	yes
40	HD42B	$e^- + p^+ + *OCH_3 \rightleftharpoons CH_3OH + *$	yes	yes	yes
41	H41A	$e^- + p^+ + *CH_2OH \rightleftharpoons *CH_2 + H_2O$	yes	yes	yes

42	HD41A	$e^- + p^+ + **CH_2OH \rightleftharpoons CH_3OH + 2*$	yes	yes	yes
43	HD42A	$e^- + p^+ + *OCH_3 \rightleftharpoons CH_4 + *O$	yes	yes	yes
44	H05B	$e^- + p^+ + *COH \rightleftharpoons *CHOH$	yes	yes	yes
45	C03Ai	$*CO + *CO \rightleftharpoons **OCCO$	no	no	no
46	C03Aii	$*CO + *CO \rightleftharpoons **(CO)_2$	no	no	no
47	H16Ai	$e^- + p^+ + **OCCO \rightleftharpoons **COHCO$	yes	yes	yes
48	H14Ai	$e^- + p^+ + **COHCO \rightleftharpoons *CCO + H_2O + *$	yes	yes	yes
49	H14Aii	$e^- + p^+ + **COCOH \rightleftharpoons *CCO + H_2O + *$	yes	yes	yes
50	H16Aii	$e^- + p^+ + **(CO)_2 \rightleftharpoons **COCOH$	yes	yes	yes
51	H19A	$e^- + p^+ + *CCO \rightleftharpoons *CHCO$	yes	yes	yes
52	H58A	$2* + e^- + p^+ + *CHCO \rightleftharpoons ***CH_2CO$	yes	yes	yes
53	H59A	$e^- + p^+ + ***CH_2CO \rightleftharpoons **OCHCH_2 + *$	yes	yes	yes
54	H53B	$e^- + p^+ + **OCHCH_2 \rightleftharpoons **CH_2OCH_2$	yes	yes	yes
55	H80A	$e^- + p^+ + **CHCH_2O \rightleftharpoons **CH_2OCH_2$	yes	yes	yes
56	H79A	$e^- + p^+ + **CHOHCH_2O \rightleftharpoons **CHCH_2O + H_2O$	yes	yes	yes
57	H71A	$e^- + p^+ + **COHCH_2O \rightleftharpoons **CHOHCH_2O$	yes	yes	yes
58	O71A	$**COHCH_2O \rightleftharpoons *COHCH_2O + *$	no	no	no
59	HD77A	$e^- + p^+ + *COHCH_2O \rightleftharpoons CH_3COOH + *$	yes	yes	yes
60	H70A	$e^- + p^+ + **COCH_2O \rightleftharpoons **COHCH_2O$	yes	yes	yes
61	O69A	$**COCHOH \rightleftharpoons **COCH_2O$	no	no	no
62	H17Ai	$* + e^- + p^+ + *COCHO \rightleftharpoons **COCHOH$	yes	yes	yes
63	H16Bi	$e^- + p^+ + **(CO)_2 \rightleftharpoons *COCHO + *$	yes	yes	yes
64	H16Bii	$e^- + p^+ + **(CO)_2 \rightleftharpoons **COCHO$	yes	yes	yes
65	H17Aii	$e^- + p^+ + **COCHO \rightleftharpoons **COCHOH$	yes	yes	yes
66	C03Bi	$*CO + *CHO \rightleftharpoons *COCHO + *$	no	no	no
67	C03Bii	$*CO + *CHO \rightleftharpoons **COCHO$	no	no	no
68	H51Ai	$e^- + p^+ + **OCHCH \rightleftharpoons **OCHCH_2$	yes	yes	yes
69	H49B	$e^- + p^+ + **CHOCHOH \rightleftharpoons **OCHCH + H_2O$	yes	yes	yes
70	H49C	$e^- + p^+ + **CHOCHOH \rightleftharpoons **CHOCH_2OH$	yes	yes	yes
71	H73B	$e^- + p^+ + **CHOCH_2OH \rightleftharpoons *OCHCH_2 + H_2O + *$	yes	yes	yes
72	O53A	$**OCHCH_2 \rightleftharpoons *OCHCH_2 + *$	no	no	no
73	H51Aii	$e^- + p^+ + **OCHCH \rightleftharpoons *OCHCH_2 + *$	yes	yes	yes
74	C04A	$*CHO + *CHO \rightleftharpoons **CHOCHO$	no	no	no
75	H48A	$e^- + p^+ + **CHOCHO \rightleftharpoons **CHOCHOH$	yes	yes	yes
76	D45A	$**CH_2OCH_2 \rightleftharpoons C_2H_4 + *O + *$	no	no	no
77	H45B	$e^- + p^+ + **CH_2OCH_2 \rightleftharpoons **OHCH_2CH_2$	yes	yes	yes
78	D47A	$**OHCH_2CH_2 \rightleftharpoons C_2H_4 + *OH + *$	no	no	no
79	CD35A	$*CH_2 + *CH_2 \rightleftharpoons C_2H_4 + 2*$	no	no	no
80	H92A	$e^- + p^+ + *O \rightleftharpoons *OH$	yes	yes	yes
81	HD93A	$e^- + p^+ + *OH \rightleftharpoons H_2O + *$	yes	yes	yes
82	H53Aii	$* + e^- + p^+ + *OCHCH_2 \rightleftharpoons **CHOHCH_2$	yes	yes	yes
83	H54B	$e^- + p^+ + **CHOHCH_2 \rightleftharpoons *CH_2CH_2OH + *$	yes	yes	yes
84	HD47Aii	$e^- + p^+ + *CH_2CH_2OH \rightleftharpoons CH_3CH_2OH + *$	yes	yes	yes
85	HD47Ai	$e^- + p^+ + **OHCH_2CH_2 \rightleftharpoons CH_3CH_2OH + 2*$	yes	yes	yes
86	H53Ai	$e^- + p^+ + **OCHCH_2 \rightleftharpoons **OHCHCH_2$	yes	yes	yes
87	H54A	$e^- + p^+ + **OHCHCH_2 \rightleftharpoons **CHCH_2 + H_2O$	yes	yes	yes
88	HD55A	$e^- + p^+ + **CHCH_2 \rightleftharpoons C_2H_4 + 2*$	yes	yes	yes

B Reaction parameter values and ranges

Gibbs free energies, activation barriers and charge transfer coefficient are needed for the kinetic modelling of reactions described in section A. They were mostly obtained from the literature where ab initio DFT calculations were carried out. Some of the values had to be converted according to

$$E_{\mathrm{act}}(U) = E_{\mathrm{act}}(U^\circ) + \beta' \cdot (U - U^\circ) \tag{B.1}$$
$$E_{\mathrm{act}}(0\,\mathrm{V}) = E_{\mathrm{act}}(U^\circ) - \beta' \cdot U^\circ. \tag{B.2}$$

B.1 Confidence intervals

We based the ranges in which we allowed reaction parameters to vary on confidence in and uncertainties of DFT values used. Tab. 2 shows systematic errors and uncertainties expected of DFT calculations.

Table 2: *Uncertainties related to DFT calculations*

Nr.	type	value	uncertainty	error source	incorporated?	reference
1	β	unknown	0.5 ± 0.2	asymmetry		[24]
2	E_{act}	known	0.01 to 0.27	solvation	yes	[24]
3	β	known	0.01 to 0.05	solvation	yes	[24]
4	E_{act}	known	≈ 0.03	layers	yes	[24]
5	β	known	≈ 0.01	no. of layers	yes	[24]
6	ΔG	known	≈ 0.03	no. of layers	yes	[24]
7	ΔG	known	0.2 to 0.8	$*$CO coverage	partially	[23]
8	ΔG	known	≈ 0.2	DFT in general	no	[23]
9	E_{act}	known	≈ 0.2	DFT in general	no	[23]
10	ΔG	known	≤ 0.24	U (CEP vs. CHE)	partially	[11]
11	E_{act}	known	≤ 0.21	U (CEP vs. CHE)	partially	[11]
12	E_{act}	known	≤ 0.34	PMF error prop	no	[5]
13	ΔG	known	≤ 0.36	PMF error prop	no	[5]
14	ΔG	known	0.11 to 0.14	solvation	no	[12]
15	U_0	known	≈ 0.09	vs. experiment	no	[12]
16	E_{act}	known	0.05 to 0.30	$*$CO coverage	partially	[32]
17	ΔG	known	≤ 0.5	systemic errors		[7]
18	ΔG	unknown	$\approx \pm 0.2$	OCO backbone		[7]
19	ΔG	unknown	$\approx \pm 0.1$	C=O bond		[7]
20	μ	known	≈ 0.02	Temperature		[36]
21	μ	known	≈ 0.01	imprecision		[36]

Based on these, we came up with different confidence types that are tied to uncertainty ranges:

- For Gibbs free energies ΔG with good confidence we still have to consider uncertainties Nr. 8 and 17, resulting in ranges of minimum $\pm 0.1\,\mathrm{eV}$ and maximum $\pm 0.25\,\mathrm{eV}$. If values on a specific reaction are conflicting or if data is not available on this specific reaction and/or facet and has to be derived from others, all the other uncertainties can come into play: We therefore assume uncertainty ranges from $\pm 0.5\,\mathrm{eV}$ and maximum $\pm 1.0\,\mathrm{eV}$ in this case.

- Electrochemical potentials μ included in the MKM are all tabulated values that are very precise and only include minor uncertainties Nr. 20 and 21. In order to give some leeway for unclear product phases etc. we round up and assume uncertainty ranges of $\pm 0.05\,\mathrm{eV}$

- Activation barriers E_{act} with high confidence exhibit only general uncertainties Nr. 9, 11 and 12, resulting in ranges of minimum $\pm 0.1\,\mathrm{eV}$ and maximum $\pm 0.2\,\mathrm{eV}$. For values that we have less confidence in, thee might add up and also uncertainties Nr. 2, 4 and 16 can come into play. We therefore assume uncertainty ranges from $\pm 0.2\,\mathrm{eV}$ and maximum $\pm 0.3\,\mathrm{eV}$ for these. If no applicable value is available, uncertainties go beyond DFT-related considerations and we might apply ranges of up to $\pm 1.0\,\mathrm{eV}$ around some point of reference.

- For charge transfer coefficients β calculated by DFT we have to consider uncertainties Nr. 3 and 5 as well as systemic and computational errors not mentioned in the reviewed literature. For values we have a high level of confidence in we apply uncertainty ranges of $\pm 0.05\,\mathrm{eV/V}$. For values with a smaller level of confidence we assume uncertainty ranges from minimum $\pm 0.1\,\mathrm{eV/V}$ up to a maximum $\pm 0.15\,\mathrm{eV/V}$.
  If there is no available charge transfer coefficient for a reaction we can always assume the perfectly symmetrical case of $\beta = 0.5\,\mathrm{eV/V}$ based on uncertainty Nr. 1. The uncertainty ranges add up to $\pm 0.25\,\mathrm{eV/V}$.

B.2 Parameters from DFT

In section B.1 we derived general confidence intervals. The actual target values and uncertainty ranges used are shown in Tab. 3. Based on literature data as well as the consistency within and across different sources, target values and confidence intervals were defined. For the calibrated model we aimed to use parameters as close as possible to the defined targets and stay within the ranges as a hard boundary condition. For some reactions, data availability was so scarce or exclusive to other facets that we only defined a range without a target value based on the information available.

Table 3: *All considered DFT data reported on reaction parameters.*

reaction	$\Delta G^{\ominus}$ [eV] chosen	alternatives	range		E_{act} [eV] chosen	alternatives	range		β [eV/V] chosen	alternatives	range	
AH01A	0.59[5, 9]	0.60[l,j]	0.49	0.69	0.92[24]	0.80[l,j]	0.65	1.05	0.44[24]	0.45[jl]	0.34	0.54
A01A	0.32[5]	1.03[j][38]	0.12	0.52	0.43[5]	0.46[38][j] 0.63[a][5]	0.30	0.70	0.50[h]	0.82[j][38]	0.25	0.75
A01B	-	0.32[g][5] 0.33[k][23]	0.13	0.53	0.43[5]	-0.28[k][23] 0.63[a][5]	0.30	0.70	n.a.		-	-
H06A	0.27[c][5]	-0.71[j][38] -0.02[k][23]	0.07	0.47	0.37[5]	0.57[a][5]	0.10	0.90	0.50[h]		0.25	0.75
AH01B	-0.05[9]	0.25[jl][9, 38] -0.35[l][9, 30][k]	-0.25	0.15	1.00[h]		0.00	2.00	0.50[h]		0.25	0.75
HD07A	-	0.46[j][38]	0.00	1.00	1.50[h]		0.00	2.00	0.50[h]		0.25	0.75
C03Ai	1.01[24]	1.19[4]	0.90	1.30	1.06[24]	1.26[4]	0.86	1.26	n.a.	0.68[4]	-	-
C03Aii	0.21[i] [11]		0.01	0.41	0.53[12]	0.45[32]	0.43	0.63	n.a.	0.17[12]	-	-
H82B	-	0.00[j][38]	-1.00	1.00	0.80[h]	0.38[j][38]	0.00	2.00	0.50[h]	1.15[j][38]	0.25	0.75
H02A	-0.55[b][5]	-0.12[g][5] -0.48[j][27] -0.44[k][23]	-0.75	-0.35	0.50[a][5]	0.88[24] 0.30[5] 0.80[j][26, 27]	0.20	1.00	0.52[24]	0.52[j][26, 27]	0.42	0.62
A13A	-0.59[11]	-0.75[22] -0.25[12] -0.40[jl][22, 38]	-0.75	-0.25	0.20[h]	-0.06[k][23]	0.00	2.00	n.a.		-	-
H03A	0.62[24]	0.37[22] 0.65[11] 0.71[i][11] 1.35[12]	0.57	0.67	0.64[24]	0.87[22] 0.55[6]	0.54	0.74	0.53[24]	0.50[11, 22] 0.78[12]	0.48	0.58
H16Ai	0.20[24]		0.00	0.40	0.59[24]		0.39	0.79	0.48[24]		0.38	0.58
H16Aii	-	0.48[k][23]	0.00	1.00	-	0.64[k][23]	0.20	1.00	0.50[h]		0.25	0.75
A98B(a)	0.11[22]	0.03[l][24]	0.01	0.21	1.50[h]		0.00	2.00	0.80[22]	0.40[j][22]	0.7	0.9

		0.19[29] 0.12^{j}[22] -0.02^{k}[22]							0.70^{k}[22]			
A98B(h)			-0.50	1.50	1.54^{k}[23]		0.50	2.50	0.50^{h}		0.25	0.75
H03B	0.74[22, 24]	1.07[6] 0.65^{jl}[27, 39] 1.40^{jkl}[22, 23, 39]	0.64	0.84	0.92[24]	0.65^{jl}[26, 27, 39] 1.45^{kl}[22, 23]	0.72	1.12	0.46[24]	0.45^{j}[26, 27] 0.50[22]	0.41	0.51
HD96A(a)	-0.11[22]	-0.12^{j}[22] -0.05^{kl}[22, 23]	-0.21	-0.01	-	1.80^{k}[23]	1.00	3	0.50[22]	0.50^{k}[22] 1.00^{j}[22]	0.4	0.6
HD96A(h)	-		-0.50	1.50	1.53[12]		1.33	1.73	0.80[12]		0.70	0.90
HD96A(t)	-0.22[22]	-0.24^{j}[22] -0.10^{kl}[22, 23]	-0.42	-0.02	-	0.80^{k}[23]	0.00	2	n.a.		-	-
H05A	-0.16[24]	0.98^{j}[27]	-0.36	0.04	1.00[24]		0.80	1.20	0.46[24]		0.36	0.56
H33A	-0.36[24]	-1.10^{j}[27]	-0.56	-0.16	0.84[24]		0.64	1.04	0.50[24]		0.40	0.60
H34A	0.08[24]	0.17[6]	-0.12	0.28	0.66[24]		0.46	0.86	0.49[24]	0.50[22]	0.44	0.54
H35A	-0.56[24]	0.00[6]	-0.76	-0.36	0.69[24]		0.49	0.89	0.49[24]	0.50[22]	0.44	0.54
HD36A	-1.57[24]	-0.60^{l}	-1.70	-0.70	0.79[24]		0.59	0.99	0.50[24]	0.50[22]	0.45	0.55
CD35A	-1.56[24]		-1.76	-1.36	0.46[24]		0.26	0.66			-	-
H04B	-0.23[24]	0.51^{ge}[6]	-0.43	-0.03	0.49[24]	1.01^{eg}[6]	0.29	0.69	0.51[24]		0.41	0.61
H39B	-0.40[24]	-0.45^{j}[27]	-0.60	-0.20	0.63[24]		0.43	0.83	0.48[24]		0.38	0.58
HD42A	-1.30[24]		-1.50	-1.10	2.58[24]		2.38	2.78	0.40[24]		0.30	0.50
HD42B	-0.09[24]	-0.29^{j}[27]	-0.									
11	1.03[24]		0.83	1.23	0.45[24]		0.35	0.55				
C04A	-1.19[24]		-1.39	-0.99	0.22[24]		0.02	0.42	n.a.		-	-
H48A	0.35[24]	0.01[11] 0.14^{i}[11]	-0.15	0.85	0.97[24]		0.77	1.17	0.47[24]		0.37	0.57
H49B	-0.85[24]		-1.05	-0.65	0.92[24]		0.72	1.12	0.46[24]		0.36	0.56
H49C	-0.5[11]	-0.36^{i}[11]	-0.70	-0.30	0.60^{h}		0.00	2.00	0.50[24]		0.40	0.60
H73B	-0.85[11]	-0.77^{i}[11]	-1.05	-0.65	0.60^{h}		0.00	2.00	0.50[24]		0.40	0.60
H51Ai	-0.1[24]		-0.30	0.10	0.75[24]		0.55	0.95	0.48[24]		0.38	0.58

H51Aii	-		-1.00	1.00	0.60[h]		0.00	2.00	0.50[h]	0.25	0.75
H53Ai	0.44[24]		0.24	0.64	0.90[24]		0.70	1.10	0.49[24]	0.39	0.59
H53Aii	0.12[11]	0.26[i][11]	-0.08	0.32	0.60[h]		0.00	2.00	0.50[11]	0.40	0.60
O53A	-0.42[11]	-0.46[i][11]	-0.62	-0.22	0.30[h]		0.00	2.00	n.a.	-	-
H54A	0.11[24]		-0.09	0.31	1.10[24]		0.90	1.30	0.53[24]	0.43	0.63
HD55A	-0.96[24]		-1.16	-0.76	0.50[24]		0.30	0.70	0.47[24]	0.37	0.57
H53B	0.06[24]		-0.14	0.26	0.83[24]		0.63	1.03	0.52[24]	0.42	0.62
H45B	0.18[24]		-0.02	0.38	0.84[24]		0.64	1.04	0.49[24]	0.39	0.59
D45A	0.05[24]	-0.75[11]	-0.95	1.05	1.01[24]		0.81	1.21	n.a.	-	-
H92A	-0.52[c][24]		-1.00	1.00	0.30[h]		0.00	2.00	0.50[h]	0.25	0.75
HD93A	0.00[c][24]		-1.00	1.00	0.30[h]		0.00	2.00	0.50[22]	0.40	0.60
D47A	-0.65[24]		-0.85	-0.45	0.39[24]		0.19	0.59	n.a.	-	-
HD47Ai	-0.54[24]		-1.00	0.00	0.75[24]		0.55	0.95	0.52[24]	0.42	0.62
HD47Aii	-0.82[11]	-0.61[i][11]	-1.02	-0.62	0.60[h]		0.00	2.00	0.50[11]	0.40	0.60
H14Ai	-1.59[24]		-1.79	-1.39	0.35[24]		0.15	0.55	0.50[24]	0.40	0.60
H14Aii	-	-0.78[k][23]	-1.28	-0.28	-	0.28[k][23]	0.00	0.60	0.50[h]	0.25	0.75
H19A	0.31[24]	-0.68[k][23]	0.11	0.51	1.02[24]		0.82	1.22	0.48[24]	0.38	0.58
H58A	0.03[24]		-0.17	0.23	1.00[24]		0.80	1.20	0.47[24]	0.37	0.57
H59A	-0.51[24]		-0.71	-0.31	0.61[24]		0.41	0.81	0.48[24]	0.38	0.58
D39A	-0.03[k][23]	0.51[ge][6]	-0.50	0.50	0.30[h]	1.01[eg][6]	0.00	2.00	n.a.	-	-
H04A	0.39[24]	0.26[22] 0.05[6] 0.43[j][22] 0.40[kl][22, 23]	0.25	0.45	0.98[24]		0.78	1.18	0.50[22] 0.47[24]	0.42	0.52
H05B	0.27[c][24]	-0.11[22]	-0.23	0.77	1.62[22]		1.42	1.82	0.50[22]	0.40	0.60
H38A	-0.79[c][24]		-1.04	-0.54	0.63[24]		0.43	0.83	0.50[22]	0.40	0.60
H38B	-0.34[c][24]		-0.59	-0.09	-	0.39[j][27][26]	0.10	0.80	0.50[h]	0.25	0.75
H39Ai	0.28[24]	0.66[dj][26, 27] 1.01[ej][26, 27]	0.08	0.48	0.98[24]		0.78	1.18	0.48[24]	0.38	0.58

H39Aii	-	-0.06[k][23]	-0.5	0.50	-	1.10[k][23]	0.90	1.30	0.50[h]		0.25	0.75
HD41A	-0.77[c][24]		-1.27	-0.27	-	0.42[j][26]	0.00	0.80	0.50[h]		0.25	0.75
H41A	-0.37[gc][24]		-0.87	0.13	-	1.18[k][23]	0.80	1.60	0.50[h]		0.25	0.75
A95A	0.06[12]		-0.14	0.26	0.60[h]		0.00	2.00	n.a.		-	-
O93A	1.06[12]		0.86	1.26	0.68[12]		0.48	0.88	0.42[12]		0.32	0.52
C03Bi	-0.33[11]	-0.37[i][11] -0.12[j][11]	-0.54	-0.13	0.77[24]	0.63[12]	0.62	0.82	n.a.	0.08[12]	-	-
C03Bii	-	0.45[k][23]	-1.55	1.45	-	1.47[k][23]	1.00	1.80	n.a.		-	-
H16Bi	-		-1.00	1.00	0.97[24]	0.43[12]	0.20	1.20	0.51[24]	0.17[12]	0.15	0.55
H16Bii	$\bar{0}$.26[kf][23]	0.16[k][23]	-0.24	0.76	$\bar{1}$.31[kf][23]	1.00[ek][23]	0.50	1.50	0.50[h]		0.15	0.55
H17Ai	0.31[11]	0.39[i][11]	0.11	0.51	0.78[11]		0.58	0.98	0.50[11]	0.29[c][11]	0.25	0.55
H17Aii	-	-0.04[kc][23]	-0.54	0.46	0.60[h]		0.00	2.00	0.50[h]		0.25	0.75
O69A	-0.64[11]	-0.62[i][11]	-0.84	-0.44	0.19[11]		0.00	0.39	n.a.		-	-
H70A	0.44[11]	0.68[i][11]	0.19	0.69	0.60[h]		0.00	2.00	0.50[c][11]		0.40	0.60
O71A	0.52[11]	0.46[i][11]	0.32	0.72	0.30[h]		0.00	2.00	n.a.		-	-
HD77A	-2.97[11]	-2.72[i][11]	-3.22	-2.72	0.60[h]		0.00	2.00	0.50[c][11]		0.40	0.60
H71A	-0.72[11]	-0.96[i][11]	-0.97	-0.47	0.60[h]		0.00	2.00	0.50[c][11]		0.40	0.60
H79A	0.30[11]	0.39[i][11]	0.10	0.50	0.60[h]		0.00	2.00	0.50[c][11]		0.40	0.60
H80A	-0.85[11]	-0.74[i][11]	-1.05	-0.65	0.60[h]		0.00	2.00	0.50[c][11]		0.40	0.60
H54B	-0.03[11]	0.01[i][11]	-0.23	0.17	0.60[h]		0.00	2.00	0.50[c][11]		0.40	0.60

Some of the values are adapted:

[a] *H-shuttle hydrogenation mechanism.*

[b] *Value derived from reaction in the literature that is similar .*

[c] *Step is explicit, value is implied by thermodynamic consistency.*

[g] *Value for a similar, but not the same reaction.*

[h] *Assumed value.*

[i] *Value from calculation with CEP.*

[l] *Average of multiple values.*

Some values belong to different types of hydrogenation:

[d] *Corrected for suspected U offset.*

[e] *Tafel-style hydrogenation mechanism.*

[f] *Acidic hydrogenation mechanism.*

Some values belong to different copper facets:

[j] *Cu(111)*

[k] *Cu(211)*

B.3 Tabulated parameters

For the bulk species included in the mechanism we used well-known tabulated chemical potentials as target values [36]. These are listed in Tab. 4. Confidence intervals discussed in B.1 apply.

Table 4: *Chemical potentials of bulk species in different phases. Based on experimental observations, solubility and thermodynamic consistency, a phase was chosen for each - out of gaseous (g), liquid (l), un-ionized in aqueous solution (ao) and ionized in aqueous solution (ai).*

species	chemical potential μ [eV][36]				$c^{\mathrm{sat}}_{\mathrm{H_2O}}(298\,\mathrm{K})$	phase	
	g	l	ao	ai	$\left[\mathrm{mol\,L^{-1}}\right]$		reasoning
CO_2	-4.09	-	-4	-	3.18×10^{-2}	ao	pre-saturated electrolyte
CO	-1.42	-	-1.24	-	9.28×10^{-4}	ao	good solubility, relatively small production rates
HCOOH	-	-3.74	-3.86	-3.64	∞	ao	completely miscible, values given for protonated form
H_2	0.00	-	0.8	-	1.54×10^{-3}	g	very large production rates, bubbling observed
CH_2O	-1.06	-	-1.47	(-1.77)	$1.23e1$	g	values given for gaseous form, very volatile
CH_3OH	-1.68	-1.72	-1.82	-	∞	ao	completely miscible
CH_4	-0.53	-	-0.36	-	1.31×10^{-3}	g	large production rates, bubbling observed
CH_3COOH	-3.88	-4.04	-4.11	-3.83	∞	ao	completely miscible, values given for protonated form
CH_3CH_2OH	-1.75	-1.81	-1.88	-	∞	ao	completely miscible
C_2H_4	0.71	-	0.84	-	4.63×10^{-3}	g	large production rates

In addition, there are a few key species that take part in the reaction not as a direct educt or product. Their chemical potentials and corresponding ranges are shown in Tab. 5.

Table 5: *Additioal reactions and their Gibbs free energies used as boundary conditions for thermodynamic consistency.*

species	phase	μ [eV]	source	range	
$\cdot$	surface	0.00	assumption	0.00	0.00
e^-	solid	0.00	assumption	0.00	0.00
H_2O	liquid	-2.46	tabulated [36]	-2.51	-2.41
OH^-	liquid	-1.63	tabulated [36]	-1.68	-1.58
H^+	liquid	0.00	tabulated [36]	-0.05	0.05

For the thermodynamic calibration we included 6 additional not explicitly listed in Tab. 1 reactions with respective target values. Three of these are already included in the MKM implicitly: Volmer, Heyrovsky and Tafel steps of the HER as reactions "A98B(h)", "HD96A(h)",

and "HD96A(t)" in Tab. 3. The ones that are not part of the MKM in a straightforward manner are given in Tab. 6.

Table 6: *Additioal reactions and their Gibbs free energies used as boundary conditions for thermodynamic consistency.*

Nr.	id	reaction	$\Delta G\,[\mathrm{eV}]$	source	range	
3	water	$H_2O \rightleftharpoons H^+ + OH^-$	0.83	$pK_W = 14$	0.78	0.88
4	HER	$2\,H^+ 2\,e^- \rightleftharpoons H_2$	0.00	RHE def.[13]	0.00	0.00
13	R02A	$*COOH + e^- \rightleftharpoons *CO + OH^-$	-0.12	DFT [5]	-0.62	0.38

For the "HER" we gave no range but a single value. Together with the chemical potentials of unoccupied surface sites and electrons (see Tab.5) these are the only hard boundary conditions that we do not allow to deviate from their target values.

B.4 Pre-exponential factors

Depending on the reaction type, different pre-exponential factors (PEF) can be observed, typical ranges are shown in Tab. 7. For the model calibration, we allow parameter ranges according to adjusted values from [40] as seen in Tab. 7. For the combined reaction types with unclear assignment, we choose the smaller PEF values resp. ranges:

- For **Hydrogenation** reactions we apply PEF ranges depending on the actual mechanism:
  1. For "Heyrovsky" mechanism 1×10^5 to 1×10^{16}
  2. For "Tafel" mechanism 1×10^{11} to 1×10^{19}
  3. For "Acidic" mechanism 1×10^5 to 1×10^{16}
- For **Adsorption** reactions we apply PEF ranges of 1×10^5 to 1×10^{13}. When adsorption is coupled to a subsequent hydrogenation, the same range is used - independent of hydrogenation type.
- For sole **Desorption** reactions PEF ranges of 1×10^{12} to 1×10^{19} are used. When desorption is coupled to a prior hydrogenation, the respective ranges for hydrogenation reactions are used.
- For **Coupling** reactions PEF ranges of 1×10^{11} to 1×10^{19} are used. When they are coupled to a subsequent desorption, the same range is used.
- For **Isomerization** reactions we apply PEF ranges of 1×10^{12} to 1×10^{13}.

For all pre-exponential factors in the mechanism, we chose the Eyring coefficient at room temperature, $A = \frac{k_B T}{h} = 6.21 \times 10^{13}\,\mathrm{s}^{-1}$ as initial value.

Table 7: *Literature values of pre-exponential factors*

Name	applicable to	Unit	Krylov [19]	Baetzold [1]	Zhdanov [40]
Monomolecular reaction	O(isomerism)	s^{-1}	1×10^{10} - 1×10^{13}	1×10^{13}	1×10^{12} - 1×10^{13}
Molecular desorption	D, HD?	s^{-1}	1×10^{13}	1×10^{13}	1×10^{13} - 1×10^{19}
Associative desorption	CD	$cm^2\,s^{-1}$	1×10^{-8} - 1×10^{-1}	1×10^{-3}	1×10^{-4} - 1×10^{4}
Langmuir-Hinshelwood	C, H(t), HD(t)?, AH(t)?	$cm^2\,s^{-1}$	1×10^{-8} - 1×10^{-1}	1×10^{-3}	1×10^{-4} - 1×10^{4}
Molecular Adsorption	A, AH?	$cm^3\,s^{-1}$	1×10^{-15} - 1×10^{-11}	1×10^{-10}	1×10^{-17} - 1×10^{-10}
Eley-Rideal	H(a/h), HD(a/h)?, AH(a/h)?	$cm^3\,s^{-1}$	1×10^{-19} - 1×10^{-10}	1×10^{-10}	1×10^{-17} - 1×10^{-6}

Dimensioned parameters were adjusted to frequency factors, see Tab. 8. We used reference concentrations of liquid and surface phase to compare values within the same dimensions. The upside of focusing on Faradaic Efficiency (FE) values for calibration is that orders of magnitude need only be consistent relative to each other, not absolutely. Corrections by site concentration as in Eq. (B.3) and water concentration as in Eq. (B.4).

$$\Gamma_0 = 2.2 \times 10^{-8}\,\mathrm{kmol\,m^{-2}} = 2.2 \times 10^{-8} \frac{6 \times 10^{26}\,\mathrm{atoms}}{10\,000\,\mathrm{cm^2}} = 1.3 \times 10^{15}\,\mathrm{cm^{-2}} \approx 1 \times 10^{15}\,\mathrm{cm^{-2}} \tag{B.3}$$

$$c_0 = 55.5\,\mathrm{mol\,L^{-1}} = 55.5 \frac{6 \times 10^{23}\,\mathrm{atoms}}{1000\,\mathrm{cm^3}} = 3.3 \times 10^{22}\,\mathrm{cm^{-3}} \approx 1 \times 10^{22}\,\mathrm{cm^{-3}} \tag{B.4}$$

Table 8: *Adjusted literature values for frequency factors*

Name	applicable to	Unit	Krylov [19]	Baetzold [1]	Zhdanov [40]
Monomolecular reaction	O(isomerism)	s^{-1}	1×10^{10} - 1×10^{13}	1×10^{13}	1×10^{12} - 1×10^{13}
Molecular desorption	D, HD?	s^{-1}	1×10^{13}	1×10^{13}	1×10^{13} - 1×10^{19}
Associative desorption	CD	s^{-1}	1×10^{7} - 1×10^{14}	1×10^{12}	1×10^{11} - 1×10^{19}
Langmuir-Hinshelwood	C, H(t), HD(t)?, AH(t)?	s^{-1}	1×10^{7} - 1×10^{14}	1×10^{12}	1×10^{11} - 1×10^{19}
Molecular Adsorption	A, AH?	s^{-1}	1×10^{7} - 1×10^{11}	1×10^{12}	1×10^{5} - 1×10^{12}
Eley-Rideal	H(a/h), HD(a/h)?, AH(a/h)?	s^{-1}	1×10^{3} - 1×10^{12}	1×10^{12}	1×10^{5} - 1×10^{16}

C Thermodynamic Calibration

Thermodynamic consistency has to be accomplished because Gibbs free energy is a state function and therefore path-independent. We construct a Linear Equation System with with all given values and remove equations again until it is no longer overdetermined and solve it for chemical potentials. Finally, we calculate all missing ΔG and compare them to their target values. For calibration purposes, we vary the input values until minimum of objective function $\mathrm{OF} = \sum \left[(x_{\mathrm{act}} - x_{\mathrm{lit}}) / \Delta x \right]^2$ is reached, where x represents a generic result quantity. This calibration process is shown in Fig. 5 and Fig. 6.

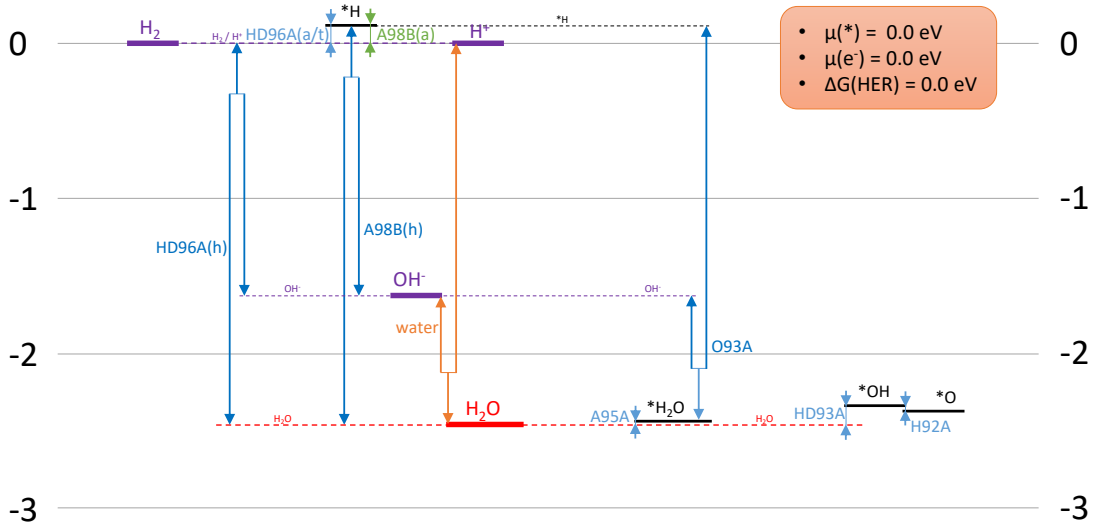

Figure 5: *Depiction of species and reaction energies, only for HER; green are given ΔG, blue are calculated ΔG, orange are given ΔG that are not included in the mechanism but used for sanity-checking; Red are given μ, black are calculated μ, purple are calculated μ where a given value is used for sanity-check*

Multiple thermodynamic parameter sets of chemical potentials were calibrated as seen in Tab. 9. The calculation of finally selected set "A5" is shown in Fig. 5 for HER and in Fig. 6 for CO2RR. All the energies of CO2RR are listed in Tab. 10 as well as Tab. 11 and depicted in a more concise way in Fig. 7.

Table 9: *Calibrated parameter sets with OF values and other key indicators.*

Name	Root mean-squared error	average target distance	average range distance
A5	9.218	0.078	0.000
F2	5.477	0.051	0.011
G1	11.894	0.075	0.002

Table 10: *Gibbs free energies for all involved reactions of our MKM after thermodynamic calibration. The rightmost columnn indicates if the respective value was used as a given boundary condition or not.*

ID	Name	Value	Target	range		given?
1	A98B(a)	0.117	0.110	0.010	0.210	yes
2	A95A	-0.026	0.060	-0.140	0.260	yes
3	water	0.830	0.830	0.780	0.880	yes
4	HER	0.000	0.000	0.000	0.000	yes
5	O93A	0.973	1.060	0.860	1.260	no
6	A98B(h)	0.947	0	-0.500	1.500	no
7	HD96A(h)	0.713	0	-0.500	1.500	no
8	HD96A(a)	-0.117	-0.110	-0.210	-0.010	no
9	HD96A(t)	-0.234	-0.220	-0.420	-0.020	no
10	AH01A	0.588	0.590	0.490	0.690	yes
11	A13A	-0.298	-0.50	-0.750	-0.250	yes
12	H02A	-0.573	-0.550	-0.750	-0.350	no
13	R02A	0.257	-0.120	-0.620	0.380	no
14	A01A	0.319	0.320	0.120	0.520	yes
15	H06A	0.269	0.270	0.070	0.470	no
18	A01B	0.330	0	0.130	0.530	yes
19	AH01B	-0.050	-0.050	-0.250	0.150	yes
20	H82B	-0.380	0	-1.000	1.000	no
22	HD07A	0.188	0	0.000	1.000	no
24	H03B	0.736	0.740	0.640	0.840	yes
25	H05A	-0.175	-0.160	-0.360	0.040	yes
26	H33A	-0.378	-0.360	-0.560	-0.160	yes
27	H34A	0.043	0.080	-0.120	0.280	yes
28	H35A	-0.500	-0.560	-0.760	-0.360	yes
29	HD36A	-1.194	-1.570	-1.700	-0.700	no
30	H03A	0.621	0.620	0.570	0.670	yes
31	H04B	-0.271	-0.230	-0.430	-0.030	yes
32	D39A	0.118	-0.030	-0.500	0.500	no
34	H04A	0.379	0.390	0.250	0.450	yes
35	H39Ai	0.277	0.280	0.080	0.480	yes
36	H39Aii	0.093	0	-0.500	0.500	yes
37	H38A	-0.817	-0.790	-1.040	-0.540	no
38	H38B	-0.373	-0.340	-0.590	-0.090	no
39	H39B	-0.462	-0.400	-0.600	-0.200	yes
40	HD42B	-0.177	-0.090	-0.290	0.110	no
41	H41A	-0.217	-0.370	-0.870	0.130	no
42	HD41A	-0.916	-0.770	-1.270	-0.270	no
43	HD42A	-1.276	-1.300	-1.500	-1.10	yes
44	H05B	0.264	0.270	-0.230	0.770	no
45	C03Ai	1.009	1.010	0.900	1.300	yes
46	C03Aii	0.210	0.210	0.010	0.410	yes

47	H16Ai	0.201	0.200	0.000	0.400	yes
48	H14Ai	-1.587	-1.590	-1.790	-1.390	yes
49	H14Aii	-0.936	0	-1.280	-0.280	yes
50	H16Aii	0.349	0	0.000	1.000	no
51	H19A	0.314	0.310	0.110	0.510	yes
52	H58A	0.036	0.030	-0.170	0.230	yes
53	H59A	-0.506	-0.510	-0.710	-0.310	yes
54	H53B	0.031	0.060	-0.140	0.260	yes
55	H80A	-0.900	-0.850	-1.050	-0.650	yes
56	H79A	0.250	0.300	0.100	0.500	yes
57	H71A	-0.799	-0.720	-0.970	-0.470	yes
58	O71A	0.689	0.520	0.320	0.720	yes
59	HD77A	-2.705	-2.970	-3.200	-2.700	no
60	H70A	0.628	0.440	0.190	0.690	yes
61	O69A	-0.520	-0.640	-0.840	-0.440	yes
62	H17Ai	0.429	0.310	0.110	0.510	yes
63	H16Bi	0.200	0	-1.000	1.000	no
64	H16Bii	0.291	0	-0.240	0.760	yes
65	H17Aii	0.338	0	-0.540	0.460	no
66	C03Bi	-0.211	-0.330	-0.540	-0.130	no
67	C03Bii	-0.120	0	-1.550	1.450	no
68	H51Ai	-0.116	-0.100	-0.300	0.100	yes
69	H49B	-0.865	-0.850	-1.050	-0.650	yes
70	H49C	-0.483	-0.500	-0.700	-0.300	yes
71	H73B	-0.833	-0.850	-1.050	-0.650	yes
72	O53A	-0.335	-0.420	-0.620	-0.220	no
73	H51Aii	-0.451	0	-1.000	1.000	no
74	C04A	-1.158	-1.190	-1.390	-0.990	yes
75	H48A	0.364	0.350	-0.150	0.850	no
76	D45A	-0.562	0.050	-0.950	1.050	no
77	H45B	0.121	0.180	-0.020	0.380	yes
78	D47A	-0.650	-0.650	-0.850	-0.450	yes
79	CD35A	-1.596	-1.560	-1.760	-1.360	no
80	H92A	0.033	0	-1.000	1.000	no
81	HD93A	-0.113	0	-1.000	1.000	no
82	H53Aii	0.222	0.120	-0.080	0.320	yes
83	H54B	0.074	-0.030	-0.230	0.170	yes
84	HD47Aii	-0.717	-0.820	-1.020	-0.620	no
85	HD47Ai	-0.908	-0.540	-1.000	0.000	no
86	H53Ai	0.373	0.4400	0.240	0.640	yes
87	H54A	0.043	0.110	-0.090	0.310	yes
88	HD55A	-1.027	-0.960	-1.160	-0.760	no

Table 11: *Chemical potentials of all involved species of our MKM after thermodynamic calibration. The rightmost columnn indicates if the respective value was used as a given boundary condition or not.*

ID	Name	Value	Target	range		given?
1	$*$	0.000	0.000	0.000	0.000	yes
2	e^-	0.000	0.000	0.000	0.000	yes
3	H_2O	-2.455	-2.460	-2.510	-2.410	yes
4	OH^-	-1.626	-1.630	-1.680	-1.580	no
5	H^+	0.001	0.000	-0.050	0.050	yes
6	H_2	0.002	0.000	-0.050	0.050	no
7	$*H$	0.118				no
8	$*H_2O$	-2.481				no
9	CO_2	-4.000	-4.000	-4.050	-3.950	yes
10	CO	-1.230	-1.240	-1.430	-1.230	yes
11	$*COOH$	-3.411				no
12	$*CO$	-1.528				no
13	$*CO_2^-$	-3.681				no
16	$*CO_2$	-3.670				no
17	$*OCHO$	-4.049				no
18	HCOOH	-3.860	-3.860	-3.910	-3.810	yes
20	$*COH$	-0.791				no
21	$*C$	1.490				no
22	$*CH$	1.113				no
23	$*CH_2$	1.157				no
24	$*CH_3$	0.658				no
25	CH_4	-0.535	-0.530	-0.580	-0.480	yes
26	$*CHO$	-0.906				no
27	$**CH_2O$	-1.176				no
28	CH_2O	-1.058	-1.060	-1.110	-1.010	yes
29	$*CHOH$	-0.526				no
30	$**CH_2OH$	-0.898				no
31	$*CH_2OH$	-1.082				no
32	$*OCH_3$	-1.637				no
33	CH_3OH	-1.813	-1.820	-1.870	-1.770	yes
34	$*O$	-2.377				no
35	$**OCCO$	-2.047				no
36	$**(CO)_2$	-2.846				no
37	$**COHCO$	-1.845				no
38	$*CCO$	-0.976				no
39	$**COCOH$	-2.496				no
40	$*CHCO$	-0.661				no
41	$***CH_2CO$	-0.624				no
42	$**OCHCH_2$	-1.129				no
43	$**CH_2OCH_2$	-1.097				no
44	$**CHCH_2O$	-0.198				no

45	$**CHOHCH_2O$	-2.904				no
46	$**COHCH_2O$	-2.106				no
47	$*COHCH_2O$	-1.417				no
48	CH_3COOH	-4.121	-4.110	-4.160	-4.060	yes
49	$**COCH_2O$	-2.735				no
50	$**COCHOH$	-2.215				no
51	$*COCHO$	-2.645				no
52	$**COCHO$	-2.554				no
53	$**OCHCH$	-1.014				no
54	$**CHOCHOH$	-2.605				no
55	$**CHOCH_2OH$	-3.087				no
56	$*OCHCH_2$	-1.464				no
57	$**CHOCHO$	-2.970				no
58	C_2H_4	0.718	0.710	0.650	0.750	yes
59	$**OHCH_2CH_2$	-0.975				no
60	$*OH$	-2.343				no
61	$**CHOHCH_2$	-1.241				no
62	$*CH_2CH_2OH$	-1.166				no
63	CH_3CH_2OH	-1.882	-1.880	-1.930	-1.830	yes
64	$**OHCHCH_2$	-0.755				no
65	$**CHCH_2$	1.744				no

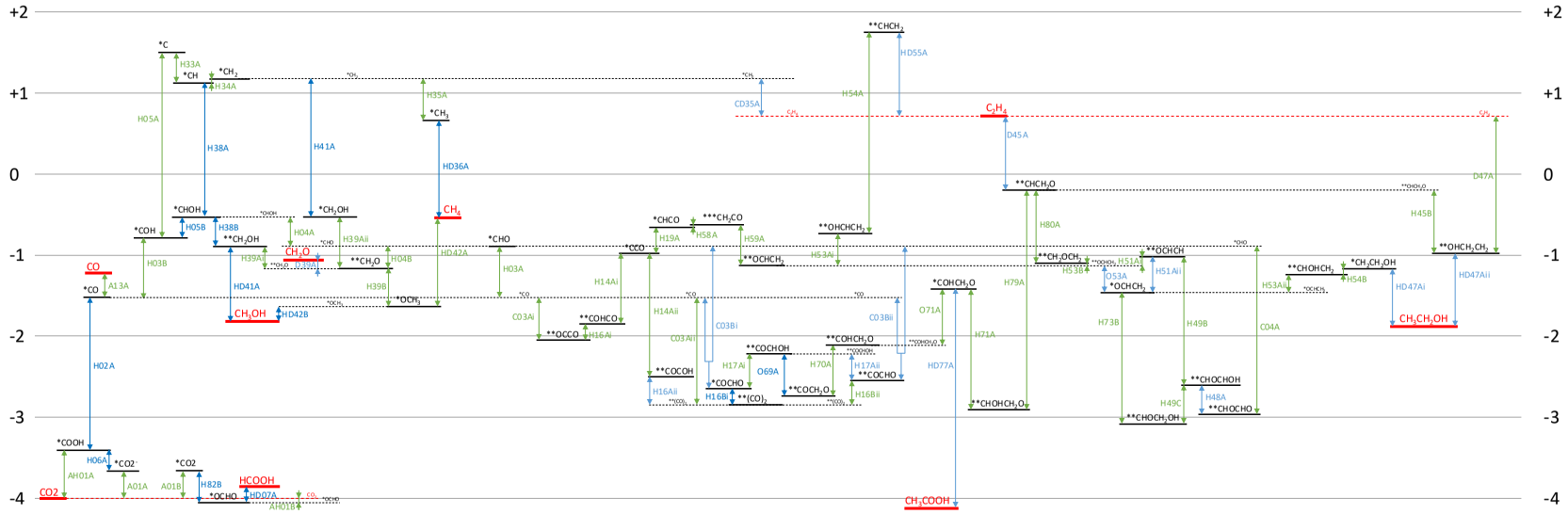

Figure 6: *Depiction of species and reaction energies, only for CO2RR; green are given ΔG, blue are calculated ΔG, orange are given ΔG that are not included in the mechanism but used for sanity-checking; Red are given μ, black are calculated μ, purple are calculated μ where a given value is used for sanity-check.*

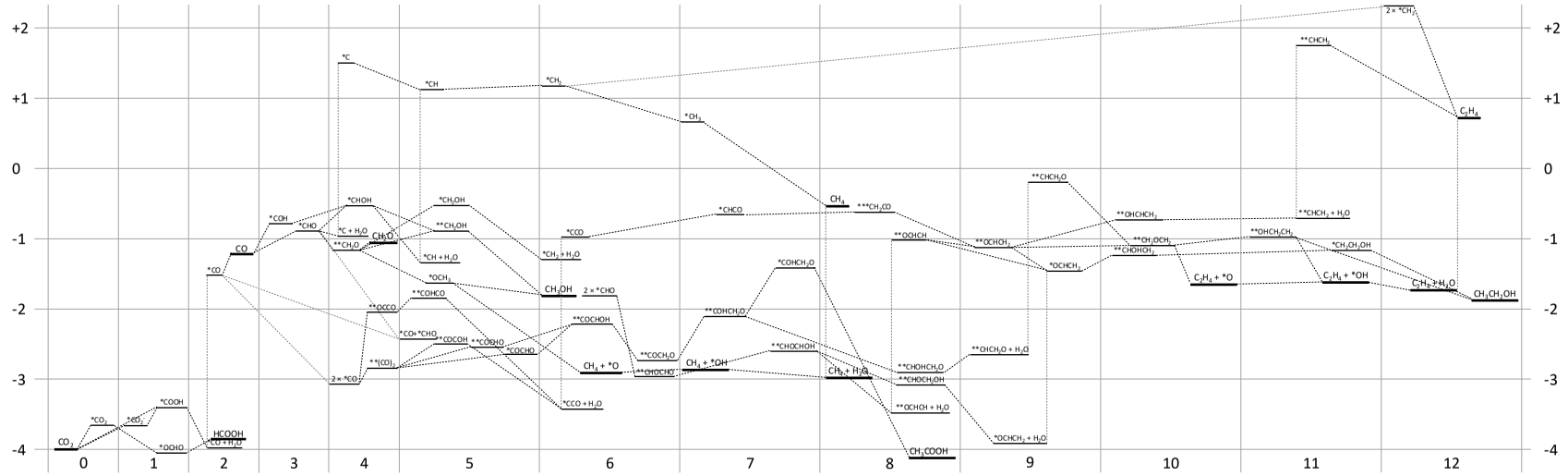

Figure 7: *Energy diagram for CO2RR from least-reduced to most-reduced state with calculated Gibbs free energies of reaction and chemical potentials of involved species.*

D Kinetic Calibration

In a first step, we slightly adjusted the reported measurement data so the sum of Faradaic Efficiencies would yield unity. We selected $\mathrm{FE}_{\mathrm{H}_2} = 1 - \sum_{k \neq 1} \mathrm{FE}_k$ because we believed hydrogen to be most likely underreported due to system escape.

We then defined a first objective function (OF) to get close to the desired regions of our parameter space. For this, logarithmically-scaled objectives are preferred because derivations around very small absolute values (e.g. $FE = 0.01$ vs. $FE = 1 \times 10^{-5}$) are punished more severely and derivations around larger absolute values (e.g. $FE = 0.5$ vs. $FE = 0.4$) less severely. We focused on the products that were actually detected by Huang and coworkers [15] and potentials where a relevant signal was detected.

The parameter space was sampled via Sobol sequence. For 10,000 points a simulation was run and objective function evaluated. The three best parameter sets were then selected. For these three parameter sets, optimizations towards the objective function were conducted using the Hooke Jeeves algorithm. With this, the OF was lowered significantly. A few very promising parameter sets emerged from this optimization, of which the most overall coherent was chosen.

A second OF was then constructed for further calibration: In order to catch more intricate qualitative trends as well as absolute values of the FE measurements, we switched to a linearly-scaled objective. On detailed inspection, the selected parameter set lead to considerable methanol production. While some methanol might have been produced undetected in the experiments considered [15], larger Faradaic Efficiencies would contradict the experimental findings. We therefore included CH_3OH as a product with $FE^{\mathrm{meas}} = 0$ throughout in the objective function.

The range of applied potential had already been narrowed down for the initial calibration described above. In order to include only evenly spaced data, one more point (at $U = -0.7\,\mathrm{V}$) was dropped for all further optimizations. The ranges used for the OF were again influenced by the standard deviations of the measurements [15]. We didn't use the actual values because this would skew the objective function very hard towards the points with very small standard deviations. The ranges were all considered as symmetrical around the measured value. Furthermore, in order to prevent numerical issues as mentioned above, we included the experimental time t_{end} at the end of our simulation in the OF. For parameter sets where numerical issues occur, the run cannot be finished within the 90 seconds of computational time given for each applied potential. By including t_{end} with the Faradaic Efficiencies, we prevent optimization in this direction. The parameter set with the lowest OF value was then analysed in more detail and manual parameter adjustments were applied. This concluded the preliminary kinetic calibration of our MKM.

Subsequently, we needed to get as close as possible to the Faradaic Efficiency of the measurement data, so we again used the linearly-scaled objective function. This time, we actually used the exact standard deviations from the measurement as uncertainty ranges wherever possible. We only made a few adjustments as to not vary more than one order of magnitude within a product and not more than two orders of magnitude across products; for the products and/or applied potentials without data, we chose the ranges accordingly. Also, t_{end} was again included with the objective function.

This time, we calibrated the pre-exponential factors of each reaction, allowing ranges according to section B.4. For this, we assumed that for hydrogenation reactions, the Eley-Rideal mechanisms (”Heyrovsky” and ”acidic”) have the same PEF and the Langmuir-Hinshelwood mechanism (”Tafel”) has a different one. We deploy the Hooke Jeeves algorithm once again and achieve another considerable reduction of the objective function.

It is evident that the quality of the model insofar as predicting Faradaic Efficiencies is higher for some potential ranges and products than others. It is also evident that some parameters influence ceratin products much more (or even much more selectively) than others. In order to conduct a final and targeted calibration, we looked at sensitivities of the Faradaic Efficiencies towards each reaction. We calculated the normalised sensitivity coefficient as has been done in similar kinetic studies [2]. In order to be able to calculate these local sensitivities, a sampling across a small slice of the parameter space was conducted. This was done via a Sobol sampling of 30,000 random points where each PEF was allowed to vary between 80% and 120% of its current value. For every single point, simulations for all 9 applied potentials were carried out.

We then selected a few key reactions towards which the products of interest have shown increased sensitivities especially for smaller applied potentials. These were the following: ”H02A”, ”A13A”, ”A98B”, ”C04A”. Since we consider these reactions with varying numbers of parameters in our model we ended up with a total of 15 parameters to calibrate. We used the same linear objective function as before and deployed the Hooke Jeeves algorithm for a last time. We were able to reduce the OF value once again for the finalized parameter set. All kinetic parametes are listed in Tab. 12.

The end result of our calibration efforts can be seen in Fig. 7.

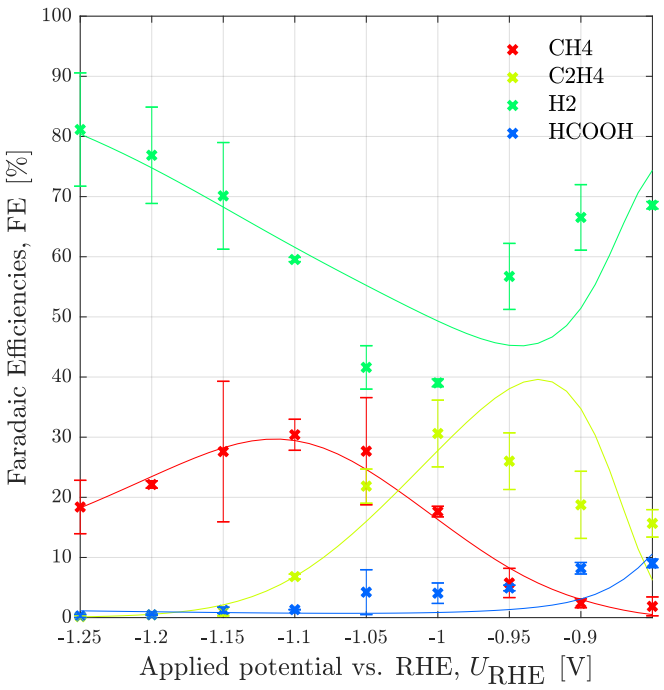

(a) Major products

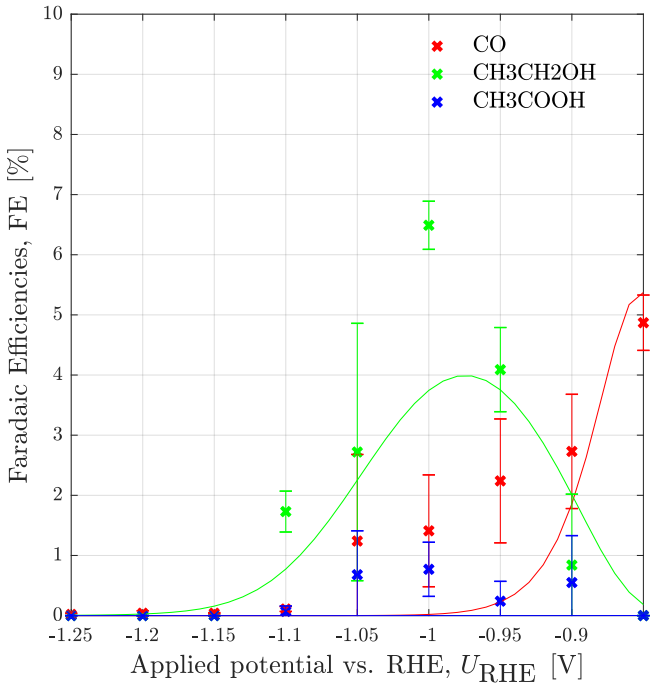

(b) Minor products

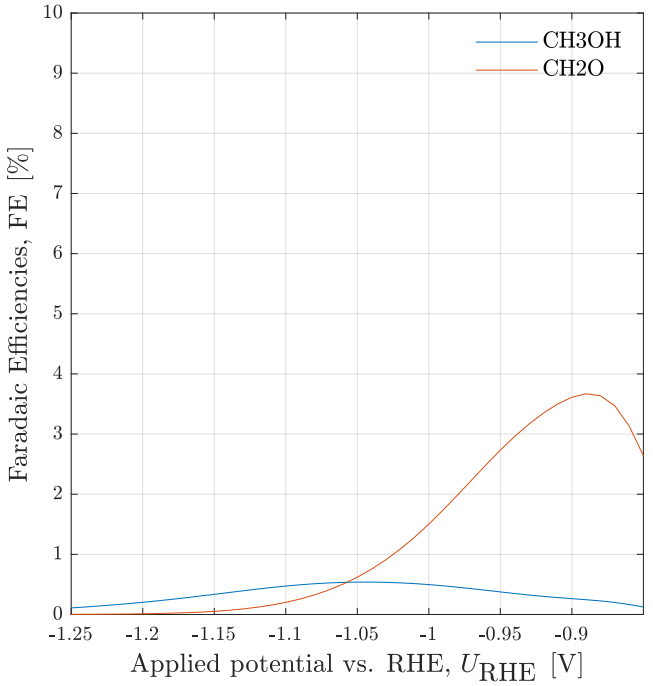

(c) Experimentally non-detected products

Figure 7: *Faradaic Efficiencies produced by the final (calibrated) MKM*

Table 12: *Kinetic parameters for all involved reactions of our MKM after final calibration.*

Nr.	ID	E_{act} [eV]				β [eV/V]				$A/A(h)/A(a)$ [s^{-1}]			$A(t)$ [s^{-1}]		
		value	target	range		value	target	range		value	range	range	value	range	
1	A98B	1.989	-	0.00	2.00	0.790	0.80	0.70	0.90	1.000×10^{13}	1×10^{5}	1×10^{13}	-		
2	A95A	0.966	-	0.00	2.00	-	-			1.000×10^{12}	1×10^{5}	1×10^{13}	-		
5	O93A	0.812	0.68	0.48	0.88	0.376	0.42	0.32	0.52	1.000×10^{12}	1×10^{11}	1×10^{19}	-		
6	A98B(h)	0.996	-	0.50	2.50	0.542	-	0.25	0.75						
7	HD96A(h)	1.532	1.53	1.33	1.73	0.730	0.80	0.70	0.90						
8	HD96A	1.330	-	1.00	3.00	0.427	0.50	0.40	0.60	2.620×10^{11}	1×10^{5}	1×10^{16}			
9	HD96A(t)	0.200	-	0.00	2.00	-	-			3.030×10^{18}	1×10^{11}	1×10^{19}			
10	AH01A	0.747	0.92	0.65	1.05	0.363	0.44	0.34	0.54	1.000×10^{13}	1×10^{5}	1×10^{13}	1.000×10^{12}	1×10^{5}	1×10^{13}
11	A13A	0.250	-	0.00	2.00	-	-			3.000×10^{12}	1×10^{5}	1×10^{13}	-		
12	H02A	0.615	0.88	0.20	1.00	0.420	0.52	0.42	0.62	1.150×10^{13}	1×10^{5}	1×10^{16}	1.680×10^{16}	1×10^{11}	1×10^{19}
14	A01A	0.493	0.43	0.30	0.70	0.455	-	0.25	0.75	6.220×10^{11}	1×10^{5}	1×10^{13}	-		
15	H06A	0.244	0.37	0.10	0.90	0.523	-	0.25	0.75	2.620×10^{11}	1×10^{5}	1×10^{16}	-		
18	A01B	0.335	0.43	0.30	0.70	-	-			2.230×10^{12}	1×10^{5}	1×10^{13}	-		
19	AH01B	1.061	-	0.00	2.00	0.585	-	0.25	0.75	1.000×10^{13}	1×10^{5}	1×10^{13}	1.000×10^{11}	1×10^{5}	1×10^{13}
20	H82B	0.180	-	0.00	2.00	0.293	-	0.25	0.75	2.620×10^{11}	1×10^{5}	1×10^{16}	6.210×10^{15}	1×10^{11}	1×10^{19}
22	HD07A	0.134	-	0.00	2.00	0.551	-	0.25	0.75	6.210×10^{12}	1×10^{5}	1×10^{16}	6.210×10^{15}	1×10^{11}	1×10^{19}
24	H03B	0.720	0.92	0.72	1.12	0.457	0.46	0.41	0.51	1.470×10^{14}	1×10^{5}	1×10^{16}	6.210×10^{18}	1×10^{11}	1×10^{19}
25	H05A	0.909	1	0.80	1.20	0.360	0.46	0.36	0.56	1.470×10^{14}	1×10^{5}	1×10^{16}	6.210×10^{18}	1×10^{11}	1×10^{19}
26	H33A	0.844	0.84	0.64	1.04	0.463	0.50	0.40	0.60	4.660×10^{8}	1×10^{5}	1×10^{16}	6.210×10^{17}	1×10^{11}	1×10^{19}
27	H34A	0.688	0.66	0.46	0.86	0.486	0.49	0.44	0.54	2.620×10^{11}	1×10^{5}	1×10^{16}	6.210×10^{16}	1×10^{11}	1×10^{19}
28	H35A	0.883	0.69	0.49	0.89	0.443	0.49	0.44	0.54	2.620×10^{11}	1×10^{5}	1×10^{16}	6.210×10^{15}	1×10^{11}	1×10^{19}
29	HD36A	0.802	0.79	0.59	0.99	0.494	0.50	0.45	0.55	4.660×10^{8}	1×10^{5}	1×10^{16}	6.210×10^{13}	1×10^{11}	1×10^{19}
30	H03A	0.546	0.64	0.54	0.74	0.483	0.53	0.48	0.58	4.660×10^{8}	1×10^{5}	1×10^{16}	6.210×10^{15}	1×10^{11}	1×10^{19}
31	H04B	0.488	0.49	0.29	0.69	0.539	0.51	0.41	0.61	6.210×10^{12}	1×10^{5}	1×10^{16}	6.210×10^{15}	1×10^{11}	1×10^{19}
32	D39A	0.197	-	0.00	2.00	-	-			1.000×10^{12}	1×10^{12}	1×10^{19}	-		
34	H04A	1.156	0.98	0.78	1.18	0.447	0.47	0.42	0.52	3.490×10^{15}	1×10^{5}	1×10^{16}	6.210×10^{15}	1×10^{11}	1×10^{19}
35	H39Ai	0.922	0.98	0.78	1.18	0.530	0.48	0.38	0.58	6.210×10^{12}	1×10^{5}	1×10^{16}	6.210×10^{13}	1×10^{11}	1×10^{19}
36	H39Aii	0.984	1.1	0.90	1.30	0.678	-	0.25	0.75	6.210×10^{12}	1×10^{5}	1×10^{16}	6.210×10^{15}	1×10^{11}	1×10^{19}
37	H38A	0.794	0.63	0.43	0.83	0.455	0.50	0.40	0.60	1.100×10^{10}	1×10^{5}	1×10^{16}	6.210×10^{16}	1×10^{11}	1×10^{19}
38	H38B	0.387	-	0.10	0.80	0.250	-	0.25	0.75	6.210×10^{12}	1×10^{5}	1×10^{16}	6.210×10^{15}	1×10^{11}	1×10^{19}

39	H39B	0.830	0.63	0.43	0.83	0.409	0.48	0.38	0.58	6.210×10^{11}	1×10^{5}	1×10^{16}	6.210×10^{14}	1×10^{11}	1×10^{19}
40	HD42B	1.156	1.03	0.83	1.23	0.520	0.45	0.35	0.55	1.100×10^{10}	1×10^{5}	1×10^{16}	6.210×10^{17}	1×10^{11}	1×10^{19}
41	H41A	1.100	-	0.80	1.60	0.550	-	0.25	0.75	1.470×10^{14}	1×10^{5}	1×10^{16}	6.210×10^{16}	1×10^{11}	1×10^{19}
42	HD41A	0.365	-	0.00	0.80	0.265	-	0.25	0.75	1.470×10^{14}	1×10^{5}	1×10^{16}	6.210×10^{16}	1×10^{11}	1×10^{19}
43	HD42A	2.780	2.58	2.38	2.78	0.330	0.40	0.30	0.50	3.490×10^{15}	1×10^{5}	1×10^{16}	6.210×10^{15}	1×10^{11}	1×10^{19}
44	H05B	1.489	1.62	1.42	1.82	0.498	0.50	0.40	0.60	1.100×10^{10}	1×10^{5}	1×10^{16}	6.210×10^{16}	1×10^{11}	1×10^{19}
45	C03Ai	1.071	1.06	0.86	1.26	-	-			6.000×10^{16}	1×10^{11}	1×10^{19}	-		
46	C03Aii	0.430	0.53	0.43	0.63	-	-			6.000×10^{16}	1×10^{11}	1×10^{19}	-		
47	H16Ai	0.412	0.59	0.39	0.79	0.462	0.48	0.38	0.58	3.490×10^{15}	1×10^{5}	1×10^{16}	6.210×10^{15}	1×10^{11}	1×10^{19}
48	H14Ai	0.550	0.35	0.15	0.55	0.590	0.50	0.40	0.60	1.100×10^{10}	1×10^{5}	1×10^{16}	6.210×10^{15}	1×10^{11}	1×10^{19}
49	H14Aii	0.363	-	0.00	0.60	0.596	-	0.25	0.75	6.210×10^{12}	1×10^{5}	1×10^{16}	6.210×10^{15}	1×10^{11}	1×10^{19}
50	H16Aii	1.000	-	0.20	1.00	0.275	-	0.25	0.75	2.620×10^{11}	1×10^{5}	1×10^{16}	6.210×10^{15}	1×10^{11}	1×10^{19}
51	H19A	0.940	1.02	0.82	1.22	0.573	0.48	0.38	0.58	3.490×10^{15}	1×10^{5}	1×10^{16}	6.210×10^{15}	1×10^{11}	1×10^{19}
52	H58A	1.067	1.00	0.80	1.20	0.485	0.47	0.37	0.57	6.210×10^{12}	1×10^{5}	1×10^{16}	6.210×10^{15}	1×10^{11}	1×10^{19}
53	H59A	0.410	0.61	0.41	0.81	0.509	0.48	0.38	0.58	2.620×10^{11}	1×10^{5}	1×10^{16}	6.210×10^{15}	1×10^{11}	1×10^{19}
54	H53B	0.916	0.83	0.63	1.03	0.443	0.52	0.42	0.62	6.210×10^{12}	1×10^{5}	1×10^{16}	6.210×10^{15}	1×10^{11}	1×10^{19}
55	H80A	2.000	-	0.00	2.00	0.543	0.50	0.40	0.60	6.210×10^{12}	1×10^{5}	1×10^{16}	6.210×10^{15}	1×10^{11}	1×10^{19}
56	H79A	1.606	-	0.00	2.00	0.428	0.50	0.40	0.60	6.210×10^{12}	1×10^{5}	1×10^{16}	6.210×10^{15}	1×10^{11}	1×10^{19}
57	H71A	1.820	-	0.00	2.00	0.600	0.50	0.40	0.60	1.000×10^{16}	1×10^{5}	1×10^{16}	6.200×10^{15}	1×10^{11}	1×10^{19}
58	O71A	0.240	-	0.00	2.00	-	-			8.280×10^{12}	1×10^{12}	1×10^{13}	-		
59	HD77A	0.000	-	0.00	2.00	0.514	0.50	0.40	0.60	1.470×10^{14}	1×10^{5}	1×10^{16}	6.210×10^{15}	1×10^{11}	1×10^{19}
60	H70A	0.576	-	0.00	2.00	0.576	0.50	0.40	0.60	1.470×10^{14}	1×10^{5}	1×10^{16}	6.210×10^{16}	1×10^{11}	1×10^{19}
61	O69A	0.030	0.19	0.00	0.39	-	-			6.210×10^{12}	1×10^{12}	1×10^{13}	-		
62	H17Ai	0.580	0.78	0.58	0.98	0.550	0.50	0.25	0.55	2.620×10^{11}	1×10^{5}	1×10^{16}	6.210×10^{18}	1×10^{11}	1×10^{19}
63	H16Bi	1.125	0.97	0.20	1.20	0.522	0.51	0.15	0.55	6.210×10^{12}	1×10^{5}	1×10^{16}	6.210×10^{14}	1×10^{11}	1×10^{19}
64	H16Bii	0.500	-	0.50	1.50	0.550	0.50	0.15	0.55	1.470×10^{14}	1×10^{5}	1×10^{16}	6.200×10^{14}	1×10^{11}	1×10^{19}
65	H17Aii	0.660	-	0.00	2.00	0.428	-	0.25	0.75	2.620×10^{11}	1×10^{5}	1×10^{16}	6.210×10^{13}	1×10^{11}	1×10^{19}
66	C03Bi	0.620	0.77	0.62	0.82	-	-			6.000×10^{16}	1×10^{11}	1×10^{19}	-		
67	C03Bii	1.498	-	1.00	1.80	-	-			6.000×10^{15}	1×10^{11}	1×10^{19}	-		
68	H51Ai	0.866	0.75	0.55	0.95	0.449	0.48	0.38	0.58	1.470×10^{14}	1×10^{5}	1×10^{16}	6.210×10^{15}	1×10^{11}	1×10^{19}
69	H49B	0.746	0.92	0.72	1.12	0.551	0.46	0.36	0.56	1.470×10^{14}	1×10^{5}	1×10^{16}	6.210×10^{15}	1×10^{11}	1×10^{19}
70	H49C	1.435	-	0.00	2.00	0.464	0.50	0.40	0.60	2.620×10^{11}	1×10^{5}	1×10^{16}	6.210×10^{15}	1×10^{11}	1×10^{19}
71	H73B	0.000	-	0.00	2.00	0.530	0.50	0.40	0.60	1.470×10^{14}	1×10^{5}	1×10^{16}	6.210×10^{15}	1×10^{11}	1×10^{19}
72	O53A	1.421	-	0.00	2.00	-	-			4.660×10^{12}	1×10^{12}	1×10^{13}	-		

73	H51Aii	2.000	-	0.00	3.00	0.588	-	0.25	0.75	2.620×10^{11}	1×10^{5}	1×10^{16}	6.210×10^{15}	1×10^{11}	1×10^{19}
74	C04A	0.026	0.22	0.02	0.42	-	-			1.000×10^{16}	1×10^{11}	1×10^{19}	-		
75	H48A	0.970	0.97	0.77	1.17	0.522	0.47	0.37	0.57	1.470×10^{14}	1×10^{5}	1×10^{16}	5.880×10^{12}	1×10^{11}	1×10^{19}
76	D45A	0.884	1.01	0.81	1.21	-	-			1.420×10^{13}	1×10^{12}	1×10^{19}	-		
77	H45B	0.838	0.84	0.64	1.04	0.390	0.49	0.39	0.59	1.470×10^{14}	1×10^{5}	1×10^{16}	6.210×10^{17}	1×10^{11}	1×10^{19}
78	D47A	0.449	0.39	0.19	0.59	-	-			6.000×10^{15}	1×10^{12}	1×10^{19}	-		
79	CD35A	0.272	0.46	0.26	0.66	-	-			6.000×10^{18}	1×10^{11}	1×10^{19}	-		
80	H92A	1.071	-	0.00	2.00	0.324	-	0.25	0.75	1.470×10^{14}	1×10^{5}	1×10^{16}	6.210×10^{15}	1×10^{11}	1×10^{19}
81	HD93A	0.975	-	0.00	2.00	0.564	0.50	0.40	0.60	1.470×10^{14}	1×10^{5}	1×10^{16}	6.210×10^{15}	1×10^{11}	1×10^{19}
82	H53Aii	0.800	-	0.00	2.00	0.412	0.50	0.40	0.60	6.210×10^{12}	1×10^{5}	1×10^{16}	6.210×10^{15}	1×10^{11}	1×10^{19}
83	H54B	0.390	-	0.00	2.00	0.479	0.50	0.40	0.60	2.620×10^{11}	1×10^{5}	1×10^{16}	6.210×10^{15}	1×10^{11}	1×10^{19}
84	HD47Aii	0.000	-	0.00	2.00	0.588	0.50	0.40	0.60	6.210×10^{12}	1×10^{5}	1×10^{16}	6.210×10^{15}	1×10^{11}	1×10^{19}
85	HD47Ai	0.844	0.75	0.55	0.95	0.473	0.52	0.42	0.62	6.210×10^{12}	1×10^{5}	1×10^{16}	6.210×10^{15}	1×10^{11}	1×10^{19}
86	H53Ai	1.032	0.90	0.70	1.10	0.590	0.49	0.39	0.59	6.210×10^{12}	1×10^{5}	1×10^{16}	6.210×10^{15}	1×10^{11}	1×10^{19}
87	H54A	0.900	1.10	0.90	1.30	0.630	0.53	0.43	0.63	1.470×10^{14}	1×10^{5}	1×10^{16}	6.210×10^{15}	1×10^{11}	1×10^{19}
88	HD55A	0.484	0.50	0.30	0.70	0.493	0.47	0.37	0.57	2.620×10^{11}	1×10^{5}	1×10^{16}	6.210×10^{15}	1×10^{11}	1×10^{19}

References

[1] R. C. Baetzold and G. A. Somorjai. Preexponential factors in surface reactions. *Journal of Catalysis*, 45(1):94–105, 1976. ISSN 10902694. doi:10.1016/0021-9517(76)90059-2.

[2] J. Bai, R. Geeson, F. Farazi, S. Mosbach, J. Akroyd, E. J. Bringley, and M. Kraft. Automated Calibration of a Poly(oxymethylene) Dimethyl Ether Oxidation Mechanism Using the Knowledge Graph Technology. *Journal of Chemical Information and Modeling*, 61(4):1701–1717, 2021. ISSN 15205142. doi:10.1021/acs.jcim.0c01322.

[3] Y. Y. Birdja, E. Pérez-Gallent, M. C. Figueiredo, A. J. Göttle, F. Calle-Vallejo, and M. T. Koper. Advances and challenges in understanding the electrocatalytic conversion of carbon dioxide to fuels. *Nature Energy*, 4(9):732–745, 2019. ISSN 20587546. doi:10.1038/s41560-019-0450-y.

[4] F. Calle-Vallejo and M. T. Koper. Theoretical considerations on the electroreduction of CO to C2 Species on Cu(100) electrodes. *Angewandte Chemie - International Edition*, 52(28):7282–7285, 2013. ISSN 14337851. doi:10.1002/anie.201301470.

[5] T. Cheng, H. Xiao, and W. A. Goddard. Reaction Mechanisms for the Electrochemical Reduction of CO2 to CO and Formate on the Cu(100) Surface at 298 K from Quantum Mechanics Free Energy Calculations with Explicit Water. *Journal of the American Chemical Society*, 138(42):13802–13805, 2016. ISSN 15205126. doi:10.1021/jacs.6b08534.

[6] T. Cheng, H. Xiao, and W. A. Goddard. Full atomistic reaction mechanism with kinetics for CO reduction on Cu(100) from ab initio molecular dynamics free-energy calculations at 298 K. *Proceedings of the National Academy of Sciences of the United States of America*, 114(8):1795–1800, 2017. ISSN 10916490. doi:10.1073/pnas.1612106114.

[7] R. Christensen, H. A. Hansen, and T. Vegge. Identifying systematic DFT errors in catalytic reactions. *Catalysis Science and Technology*, 5(11):4946–4949, 2015. ISSN 20444761. doi:10.1039/c5cy01332a.

[8] C. T. Dinh, T. Burdyny, G. Kibria, A. Seifitokaldani, C. M. Gabardo, F. Pelayo García De Arquer, A. Kiani, J. P. Edwards, P. De Luna, O. S. Bushuyev, C. Zou, R. Quintero-Bermudez, Y. Pang, D. Sinton, and E. H. Sargent. CO2 electroreduction to ethylene via hydroxide-mediated copper catalysis at an abrupt interface. *Science*, 360(6390):783–787, 2018. ISSN 10959203. doi:10.1126/science.aas9100.

[9] W. J. Durand, A. A. Peterson, F. Studt, F. Abild-Pedersen, and J. K. Nørskov. Structure effects on the energetics of the electrochemical reduction of CO2 by copper surfaces. *Surface Science*, 605(15-16):1354–1359, 2011. ISSN 00396028. doi:10.1016/j.susc.2011.04.028.

[10] J. T. Feaster, C. Shi, E. R. Cave, T. Hatsukade, D. N. Abram, K. P. Kuhl, C. Hahn, J. K. Nørskov, and T. F. Jaramillo. Understanding Selectivity for the Electrochemical Reduction of Carbon Dioxide to Formic Acid and Carbon Monoxide on Metal Electrodes. *ACS Catalysis*, 7(7):4822–4827, 2017. ISSN 21555435. doi:10.1021/acscatal.7b00687.

[11] A. J. Garza, A. T. Bell, and M. Head-Gordon. Mechanism of CO2 Reduction at Copper Surfaces: Pathways to C2 Products. *ACS Catalysis*, 8(2):1490–1499, 2018. ISSN 21555435. doi:10.1021/acscatal.7b03477.

[12] J. D. Goodpaster, A. T. Bell, and M. Head-Gordon. Identification of Possible Pathways for C-C Bond Formation during Electrochemical Reduction of CO2: New Theoretical Insights from an Improved Electrochemical Model. *Journal of Physical Chemistry Letters*, 7(8):1471–1477, 2016. ISSN 19487185. doi:10.1021/acs.jpclett.6b00358.

[13] A. Govind Rajan and E. A. Carter. Microkinetic model for pH- And potential-dependent oxygen evolution during water splitting on Fe-doped β-NiOOH. *Energy and Environmental Science*, 13(12):4962–4976, 2020. ISSN 17545706. doi:10.1039/d0ee02292f.

[14] Y. Hori, R. Takahashi, Y. Yoshinami, and A. Murata. Electrochemical reduction of CO at a copper electrode. *Journal of Physical Chemistry B*, 101(36):7075–7081, 1997. ISSN 15206106. doi:10.1021/jp970284i.

[15] Y. Huang, A. D. Handoko, P. Hirunsit, and B. S. Yeo. Electrochemical Reduction of CO2 Using Copper Single-Crystal Surfaces: Effects of CO Coverage on the Selective Formation of Ethylene. *ACS Catalysis*, 7(3):1749–1756, 2017. ISSN 21555435. doi:10.1021/acscatal.6b03147.

[16] R. J. Kee, C. Karakaya, and H. Zhu. Process intensification in the catalytic conversion of natural gas to fuels and chemicals. *Proceedings of the Combustion Institute*, 36(1):51–76, 2017. ISSN 15407489. doi:10.1016/j.proci.2016.06.014.

[17] B. Khezri, A. C. Fisher, and M. Pumera. CO2 reduction: The quest for electrocatalytic materials. *Journal of Materials Chemistry A*, 5(18):8230–8246, 2017. ISSN 20507496. doi:10.1039/c6ta09875d.

[18] R. Kortlever, J. Shen, K. J. P. Schouten, F. Calle-Vallejo, and M. T. Koper. Catalysts and Reaction Pathways for the Electrochemical Reduction of Carbon Dioxide. *Journal of Physical Chemistry Letters*, 6(20):4073–4082, 2015. ISSN 19487185. doi:10.1021/acs.jpclett.5b01559. URL `https://pubs.acs.org/sharingguidelines`.

[19] O. V. Krylov, M. Kisliuk, B. R. Shub, A. A. Gezalov, N. D. Maksimova, and Y. N. Rufov. No Title. *Kinetika i kataliz*, 13:598, 1972.

[20] K. P. Kuhl, E. R. Cave, D. N. Abram, and T. F. Jaramillo. New insights into the electrochemical reduction of carbon dioxide on metallic copper surfaces.

Energy and Environmental Science, 5(5):7050–7059, 2012. ISSN 17545692. doi:10.1039/c2ee21234j.

[21] A. Liu, W. Guan, Q. Cao, X. Ren, L. Gao, Q. Zhao, and T. Ma. The reaction pathway of the CO2RR to low-carbon alcohols: a theoretical study. *New Journal of Chemistry*, 44(21):8971–8976, 2020. ISSN 13699261. doi:10.1039/d0nj01265c.

[22] X. Liu, J. Xiao, H. Peng, X. Hong, K. Chan, and J. K. Nørskov. Understanding trends in electrochemical carbon dioxide reduction rates. *Nature Communications*, 8(May):1–7, 2017. ISSN 20411723. doi:10.1038/ncomms15438.

[23] X. Liu, P. Schlexer, J. Xiao, Y. Ji, L. Wang, R. B. Sandberg, M. Tang, K. S. Brown, H. Peng, S. Ringe, C. Hahn, T. F. Jaramillo, J. K. Nørskov, and K. Chan. pH effects on the electrochemical reduction of CO (2) towards C 2 products on stepped copper. *Nature Communications*, 10(1):1–10, 2019. ISSN 20411723. doi:10.1038/s41467-018-07970-9.

[24] W. Luo, X. Nie, M. J. Janik, and A. Asthagiri. Facet Dependence of CO2 Reduction Paths on Cu Electrodes. *ACS Catalysis*, 6(1):219–229, 2016. ISSN 21555435. doi:10.1021/acscatal.5b01967.

[25] J. H. Montoya, C. Shi, K. Chan, and J. K. Nørskov. Theoretical insights into a CO dimerization mechanism in CO2 electroreduction. *Journal of Physical Chemistry Letters*, 6(11):2032–2037, 2015. ISSN 19487185. doi:10.1021/acs.jpclett.5b00722.

[26] X. Nie, M. R. Esopi, M. J. Janik, and A. Asthagiri. Selectivity of CO 2 Reduction on Copper Electrodes: The Role of the Kinetics of Elementary Steps . *Angewandte Chemie*, 125(9):2519–2522, 2013. ISSN 1521-3757. doi:10.1002/ange.201208320.

[27] X. Nie, W. Luo, M. J. Janik, and A. Asthagiri. Reaction mechanisms of CO2 electrochemical reduction on Cu(1 1 1) determined with density functional theory. *Journal of Catalysis*, 312:108–122, 2014. ISSN 00219517. doi:10.1016/j.jcat.2014.01.013.

[28] S. Nitopi, E. Bertheussen, S. B. Scott, X. Liu, A. K. Engstfeld, S. Horch, B. Seger, I. E. Stephens, K. Chan, C. Hahn, J. K. Nørskov, T. F. Jaramillo, and I. Chorkendorff. Progress and Perspectives of Electrochemical CO2 Reduction on Copper in Aqueous Electrolyte. *Chemical Reviews*, 119(12):7610–7672, 2019. ISSN 15206890. doi:10.1021/acs.chemrev.8b00705. URL `https://pubs.acs.org/sharingguidelines`.

[29] J. K. Nørskov, T. Bligaard, A. Logadottir, J. R. Kitchin, J. G. Chen, S. Pandelov, and U. Stimming. Trends in the Exchange Current for Hydrogen Evolution. *Journal of The Electrochemical Society*, 152(3):J23, 2005. ISSN 00134651. doi:10.1149/1.1856988.

[30] A. A. Peterson, F. Abild-Pedersen, F. Studt, J. Rossmeisl, and J. K. Nørskov. How copper catalyzes the electroreduction of carbon dioxide into hydrocarbon fuels. *Energy and Environmental Science*, 3(9):1311–1315, 2010. ISSN 17545692. doi:10.1039/c0ee00071j.

[31] D. Ren, Y. Deng, A. D. Handoko, C. S. Chen, S. Malkhandi, and B. S. Yeo. Selective Electrochemical Reduction of Carbon Dioxide to Ethylene and Ethanol on Copper(I) oxide catalysts. *ACS Catalysis*, 5(5):2814–2821, 2015. ISSN 21555435. doi:10.1021/cs502128q.

[32] R. B. Sandberg, J. H. Montoya, K. Chan, and J. K. Nørskov. CO-CO coupling on Cu facets: Coverage, strain and field effects. *Surface Science*, 654:56–62, 2016. ISSN 00396028. doi:10.1016/j.susc.2016.08.006.

[33] K. J. P. Schouten, Z. Qin, E. P. Gallent, and M. T. Koper. Two pathways for the formation of ethylene in CO reduction on single-crystal copper electrodes. *Journal of the American Chemical Society*, 134(24):9864–9867, 2012. ISSN 00027863. doi:10.1021/ja302668n.

[34] A. H. Shah, Y. Wang, A. R. Woldu, L. Lin, M. Iqbal, D. Cahen, and T. He. Revisiting Electrochemical Reduction of CO2 on Cu Electrode: Where Do We Stand about the Intermediates? *Journal of Physical Chemistry C*, 122(32):18528–18536, 2018. ISSN 19327455. doi:10.1021/acs.jpcc.8b05348.

[35] T. K. Todorova, M. W. Schreiber, and M. Fontecave. Mechanistic Understanding of CO2 Reduction Reaction (CO2RR) Toward Multicarbon Products by Heterogeneous Copper-Based Catalysts. *ACS Catalysis*, 10(3):1754–1768, 2020. ISSN 21555435. doi:10.1021/acscatal.9b04746.

[36] D. D. Wagman, W. H. Evans, V. B. Parker, R. H. Schumm, I. Halow, S. M. Bailey, K. L. Churney, and R. L. Nuttall. The NBS tables of chemical thermodynamic properties: Selected values for inorganic and C1 and C2 organic substances in SI Units. *Journal of Physical and Chemical Reference Data*, 11, 1982. ISSN 21657254. doi:10.6028/JRES.125.007.

[37] A. Wuttig, C. Liu, Q. Peng, M. Yaguchi, C. H. Hendon, K. Motobayashi, S. Ye, M. Osawa, and Y. Surendranath. Tracking a common surface-bound intermediate during CO2-to- fuels catalysis. *ACS Central Science*, 2(8):522–528, 2016. ISSN 23747951. doi:10.1021/acscentsci.6b00155.

[38] S. Q. Xiang, S. T. Gao, J. L. Shi, W. Zhang, and L. B. Zhao. Developing micro-kinetic model for electrocatalytic reduction of carbon dioxide on copper electrode. *Journal of Catalysis*, 393:11–19, 2021. ISSN 10902694. doi:10.1016/j.jcat.2020.11.014.

[39] H. Xiao, T. Cheng, W. A. Goddard, and R. Sundararaman. Mechanistic Explanation of the pH Dependence and Onset Potentials for Hydrocarbon Products from Electrochemical Reduction of CO on Cu (111). *Journal of the American Chemical Society*, 138(2):483–486, 2016. ISSN 15205126. doi:10.1021/jacs.5b11390.

[40] V. P. Zhdanov, J. Pavlicek, and Z. Knor. Preexponential Factors for Elementary Surface Processes. *Catalysis Reviews*, 30(4):501–517, 1988. ISSN 15205703. doi:10.1080/01614948808071752.

Citation index